Utrecht University

Master Thesis

Numerical modelling of the onshore migration of Shoreward Propagating Accretionary Waves (SPAWs).

Author:
Jelmer Korteling

First Supervisor:
Dr.
Timothy Price

Second Supervisor:
Prof. dr.
Gerben Ruessink

Master Earth, Surface & Water
Physical Geography
Department of Earth Sciences
Faculty of Geosciences

July 29, 2020

Acknowledgments

I would like to thank my supervisor dr. Timothy Price for his help and guidance during this research. I would also like to thank dr. Clement Bouvier for all his help with executing the simulations and providing the needed insights on the model. Also, I would like to thank Milou to cheer me up in the lesser moments and to motivate me through the whole process. At last I would like to thank my parents Anne-Carine and Bart-Jan for always being there when I needed them.

Abstract

Recent observations have shown that the onshore return of bars is not always an alongshore-uniform process, but that horns of crescentic subtidal bars can detach and become an isolated feature in the morphology of the coast. Subsequently, it has been observed that these features can propagate shoreward as a spatially coherent structure. These fragments have been termed Shoreward Propagating Accretionary Waves (SPAWs; Wijnberg & Holman, 2007) and when they merge with the intertidal beach can act as a local natural nourishment, causing an alongshore variation in sand supply. The exact role of the onshore migration of SPAWs and the importance within the bar-beach-dune system remains unknown. Therefore, it is the aim of this paper to identify which processes control the migration of a SPAW and how this could affect the nearshore morphology, based on the numerical model 2DBeach. The results show that the migration of the SPAW is predominantly due the wave-non-linearity and that the observed circular currents provide sediment fluxes but did not contribute significantly to the onshore migration of the SPAW. A higher angle of wave incidence is not favourable for the onshore migration of a SPAW, due to the alongshore current and coinciding oblique migration path. The dimensions of the SPAW did not influence the processes regarding the onshore migration of the SPAW. However, a larger SPAW did need a longer period of time to migrate onshore. During low energetic conditions (wave height of 0.5m) the SPAW remained at its location as the waves were not high enough to break over the SPAW. When the SPAW did migrate onshore new insights were formed with respect to a trail of sand at the area the SPAW had migrated across as this has not been observed prior to this study. This implies that the SPAW loses sand over time, while migrating onshore. Therefore, a further offshore cross-shore position acts negatively to the migration success of a SPAW. On this the hypothesis is made that even though the wave conditions are favourable for the migration of a SPAW if the cross-shore distance is to far or the through is to deep the SPAW is unable to reach the inner bar or shoreline as too much sediment is lost during the migration. Due to the fact that the SPAW acts as a perturbation, the coast is more dynamically active, resulting in a faster increase in the alongshore variability than a no SPAW case. However, this does not result in a higher alongshore variability at the end of the simulation. If the SPAW does reach the inner bar or shoreline the amount of volume that the SPAW has at that moment defines the way the SPAW interacts with the existing bar-rip system. A more voluminous SPAW creates an energetic rip current at both sides of the SPAW simultaneously and creates a new bar-rip system. While, a small SPAW, on the other hand, that has lost most of its volume will solely be a nourishment for the existing bar-rip system. Summarizing, the perfect conditions for a SPAW to bring sand onshore are shore normal or slightly oblique incoming waves, which have the height to break over the SPAW.

Table of contents

1. Introduction 9

2. Literature study 10

2.1 Sandbar Dynamics 10
2.1.1 Single barred systems 10
2.1.2 Double barred systems 11
2.1.3 Bar Coupling 12
2.2.1 Definition 14
2.2.2 Initiation 14
2.2.3 Migration 14
2.2.4 Shape, frequency and lifetime 15
2.2.5 Dynamics 16

2.3 Research Question 18

3. Study site & methods 19

3.1 Study Site 19

3.2 Numerical morphodynamic model 20
3.2.1 Wave module 20
3.2.2 Circulation module 20
3.2.3 Sediment transport module 20

3.3 Model set-up 21
3.3.1 Inputs 22
3.3.2 Cases 22

3.4 Analysis & Definitions 23

4. Results 25

4.1 Base Cases 25
4.1.1 No SPAW Base Case 25
4.1.3 SPAW Base Case 26
4.1.3 Alongshore variability 30
4.1.4 Volume of the nearshore zone 31

4.2 Cross-shore location SPAW 32
4.2.1 Morphodynamics of further onshore located SPAW 32
4.2.2 Morphodynamics of further offshore located SPAW 33
4.2.3 Volume of the nearshore zone 34

4.3 SPAW dimension 35
4.3.1 Morphodynamics of a smaller SPAW 35
4.3.2 Morphodynamics of a wider SPAW 36
4.3.3 Alongshore variability 37
4.3.4 Volume of the nearshore zone 38

4.4 Wave incidence 39
4.4.1 Morphodynamics of a SPAW with oblique incoming waves 39
4.4.2 Alongshore variability 42
4.4.3 Volume of the nearshore zone 44

5. Discussion 45

5.1 SPAW morphodynamics 45
5.2 Onshore migration processes 45
5.3 Impact on nearshore morphodynamics 46
5.4 Model limitations 46
5.5 Recommendations 46

6. Conclusions 48

List of Figures

Figure 1 Classification scheme for beach morphology made by Wright and Short (1984). ..... **Fout! Bladwijzer niet gedefinieerd.**
Figure 2 Coupling patterns (Price et al., 2014). ..... **Fout! Bladwijzer niet gedefinieerd.**
Figure 3 Example of a SPAW-event (Wijnberg & Holman, 2007). 13
Figure 4 Example of a SPAW-event due to a bar bifurcation by mean(Shand, 2007). 15
Figure 5 Top view of total load transport across SPAW (b) Initial sedimentation-erosion pattern across SPAW, (c)Depth-averaged velocity pattern around the SPAW (Van der Weerd, 2012). 17
Figure 6 Location of Egmond aan Zee and the typical beach morphology (Price, 2017). 19
Figure 7 Synthetic bathymetry based on a bathymetric survey of the coast of Egmond aan Zee 22
Figure 8 Search area for tracking highest point of the SPAW 24
Figure 9 Top view of morphodynamic evolution of the coast for no SPAW base case 25
Figure 10 The evolution of the cross-shore profiles for the no SPAW base case 26
Figure 11 Top view of morphodynamic evolution of the coast and for the SPAW base case 27
Figure 12 The evolution of the cross-shore profiles for the SPAW base case 28
Figure 13 Erosion/accretion patterns over time for the SPAW base case driven 29
Figure 14 The evolution of the alongshore profile and the alongshore variability for no SPAW base case and SPAW base case 30
Figure 15 The evolution of the volume of the nearshore zone through time for no SPAW and SPAW base case 31
Figure 16 Top view of morphodynamic evolution of the coast with the start position of the SPAW located 20 meters further onshore 32
Figure 17 Top view of morphodynamic evolution of the coast with the start position of the SPAW located 20 meters further offshore 33
Figure 18 The evolution of the volume of the nearshore zone for the simulations varying the cross-shore start location of the SPAW and the no SPAW base case. 34
Figure 19 Top view of morphodynamic evolution of the coast for a SPAW with a width of 100 meters 35
Figure 20 Top view of morphodynamic evolution of the coast for a SPAW with a width of 500 meters 36
Figure 21 The evolution of the alongshore profile and alonshore variability for SPAWs with a varying width and the no SPAW base case 37
Figure 22 The evolution of the alongshore variability for SPAWs with a varying width and the no SPAW base case 38
Figure 23 The evolution of the volume of the nearshore zone for the simulations varying the width and the no SPAW base case. 39
Figure 24 Top view of morphodynamic evolution of the coast for a SPAW with the same dimensions and location as the SPAW base case, but an angle of wave incidence of 40° 40
Figure 25 Erosion/accretion patterns over time for the simulation with an angle of wave incidence of 40 ° 41

Figure 26 Migration paths of SPAWs for differing angles of wave incidence. 42
Figure 27 The evolution of the alongshore profile and alongshore variability for the simulation with an angle of wave incidence of 0°, 15° (SPAW base case) and 40°. 43
Figure 28 The evolution of the alongshore variability for the simulations with a varying angle of wave incidence 43
Figure 29 The evolution of the volume of the nearshore zone for the simulations with a varying angle of wave incidence and the no SPAW base case. 44
Figure 30 Top view of morphodynamic evolution of the coast for a SPAW with the same dimensions and location as the SPAW base case, but with a wave height of 0.5m 47

List of Tables

Table 1 Summary of conditions and SPAW characteristics at four different beaches 16
Table 2 Characteristics for all the simulations sorted by variables 23

1. Introduction

Due to wind- and wave induced processes straight and sandy coasts regularly have a strikingly alongshore variability on a range of spatial scales, differing from meters to kilometres. Throughout severe storms beach-dune systems can erode significantly, with a likewise alongshore variability in the amount of eroded sediment, due to wave induced processes (Castelle et al., 2015). Thereafter the eroded sediment gets deposited in the subtidal area. While the erosion and coinciding seaward migration of subtidal sandbars occurs during a single storm event, the recovery process of the beach-dune system is time-consuming. During the recovery the bars typically advance through the intermediate bar states towards a reflective state over a number of days to weeks (Wright and Short, 1984; Van Enckevort et al., 2004). The transition through the intermediate states coincides with a transition from a relative alongshore continuous ridge to a 3D beach morphology, due to accretive, low-steepness waves (Short, 1979; Wright and Short, 1984; Lippmann and Holman, 1990; Poate et al., 2014). This may result in a sinuous, crescentic planview of the bar morphology, which can occur in a rhythmic form in a range of wavelengths (150m – 2km) and cross-shore amplitudes (5 – 80m) (Van Enckevort et al., 2004).

Recent observations have shown that the onshore return of bars is not always an alongshore-uniform process, but that horns of crescentic subtidal bars can detach and become an isolated feature in the morphology of the coast. Subsequently, it has been observed that these features can propagate shoreward as a spatially coherent structure. These fragments have been termed Shoreward Propagating Accretionary Waves (SPAWs; Wijnberg & Holman, 2007) and when they merge with the intertidal beach can act as a local natural nourishment, causing an alongshore variation in sand supply. Additionally, it was found that SPAWs could emerge from bar bifurcations (Shand, 2007; Price et al., 2017) and in some cases erode during their onshore migration. The exact role of the onshore migration of SPAWs and the importance within the bar-beach-dune system remains unknown. So are the processes for the detachment and migration of a SPAW. It is hypothesized that high energetic conditions and the angle of wave incidence play an important role, however observations and measurements are currently lacking. Exploratory modelling results showed that wave skewness and asymmetry are a dominant factor in the onshore propagation of a SPAW. (Van der Weerd, 2012). However, it remains unknown which hydrodynamic conditions and morphology are favourable for the onshore migration of a SPAW and its welding with the beach. Therefore, it is the aim of this paper to identify which processes control the migration of a SPAW and how this could affect the nearshore morphology, based on a numerical model.

First, in Section 2 the underlying literature is discussed. Secondly the methodology and the model are introduced in Section 3. Subsequently, in Section 4 the results of the model are presented and elaborated upon. Finally, interpretations of the acquired results will be discussed in Section 5 and the main conclusions are presented in Section 6.

2. Literature study

2.1 Sandbar Dynamics

2.1.1 Single barred systems

Sandbars can be found with a high variety in spatial and temporal states, fluctuating from alongshore variable including horns an bays to alongshore uniform with a parallel bar and trough. The most widely accepted classification for single barred systems has been made by Wright and Short (1984) (Price and Ruessink, 2011; Price et al., 2014), see Figure 1. In this classification there are two end states, which are related to high and low energetic conditions and are respectively the dissipative and reflective state. In between the end states four intermediate states were identified by Wright and Short (1984), which are respectively from dissipative to reflective; longshore bar and through (LBT), rhythmic bar and beach (RBB), transverse bar and rip (TBR) and low tide terrace (LTT). Low energetic conditions make it possible to develop an alongshore variability (crescentic sandbars) which coincides with the downstate sequence towards the reflective state. The modern-day hypothesized mechanism on the subject of crescentic sandbar dynamics is the self-organizing mechanism, where there is a feedback mechanism between the morphology and hydrodynamics (Coco and Murray, 2007; Castelle et al., 2010 (a)). The basis of the mechanism is the growth of one small perturbation in the bed, triggered by feedback mechanisms between the morphology and hydrodynamics. Reduced water depth potentially leads to wave breaking that leads to an important decrease in the significant wave height and a large wave set-up. These variations in wave height can cause a cross-shore and alongshore gradients in radiation stress, leading to local set-up or set-down. The imbalance between radiation stress gradients and pressure gradients, namely residual forcing (Castelle et al., 2006; Bruneau et al., 2011; Castelle et al., 2012; Bouvier et al., 2019), indicates the net forcing available to drive nearshore currents.

In the case of two neighbouring perturbations it results in two alongshore currents meeting colliding and pushed offshore. This self-generating process results in a wave-driven circulation pattern with a narrow intense offshore flow through the bays eroding them and a wide onshore flow over the horns accreting them (Van Enckevort et al., 2004; Coco and Murray, 2007).

The duration of the downstate sequence is approximately one to multiple weeks (Van Enckevort et al., 2004). However, some sites never go through the entire sequence. Besides the development of crescentic sandbars it has been observed that during periods of low energetic conditions sandbars tend to migrate shoreward (Van Enckevoort, 2004; Van Maanen et al., 2008; Van de Lageweg et al., 2013; Castelle et al., 2010 (a); Price and Ruessink 2011). The onshore migration of sandbars during low energetic weather conditions is linked to wave non-linearity. Although, the exact mechanisms driving the onshore migration of the bars are still not fully understood.

While the downstate sequence occurs gradually, the upstate sequence, which coincides with high energetic conditions, occur on an event basis. During events of high energetic conditions all alongshore variability can be erased within hours (Van Enckevort and Ruessink, 2002(a)). The combination of high wave heights and an oblique angle of incidence induce a strong alongshore current, that can straighten out the outer bar (Ruessink, et al., 2007; Price and Ruessink, 2011). Furthermore, it has been observed that during high energetic events an offshore migration of sandbars can occur. This migration is associated with the increased wave breaking developing a potent undertow, which consequently leads to an offshore sediment transport (Gallagher et al., 1998).

In general, it has been observed that systems with larger volumes take more time to evolve through the sequences than systems with smaller volumes (Van Enckevort et al., 2014).

2.1.2 Double barred systems

A model was created by Short and Agaard (1993) that indicated that both the outer and the inner bar in a double barred system could go through the intermediate states, defined by Short and Wright (1984). It has been observed that the outer bar transforms at a slower pace through the sequence and remains in a more dissipative state than the inner bar (Ruessink, et al., 2007; Price and Ruessink, 2011).
An addition was made to the classification scheme of Wright and Short (1984) by Price and Ruessink (2011) for double barred systems. Two supplementary bar states were introduced relative to the inner and outer bar. The rhythmic low tide terrace (rLTT) state was observed for the inner bar and is characterized by a quasi-rhythmic barline and a discontinuous trough. Secondly, the erosive transverse bar and rip (eTBR) state was observed for the inner and outer bar and is characterized by the alongshore uniform barline and discontinuous through with obliquely orientated rip channels, associated with an oblique angle of wave incidence. A key element in the description of the

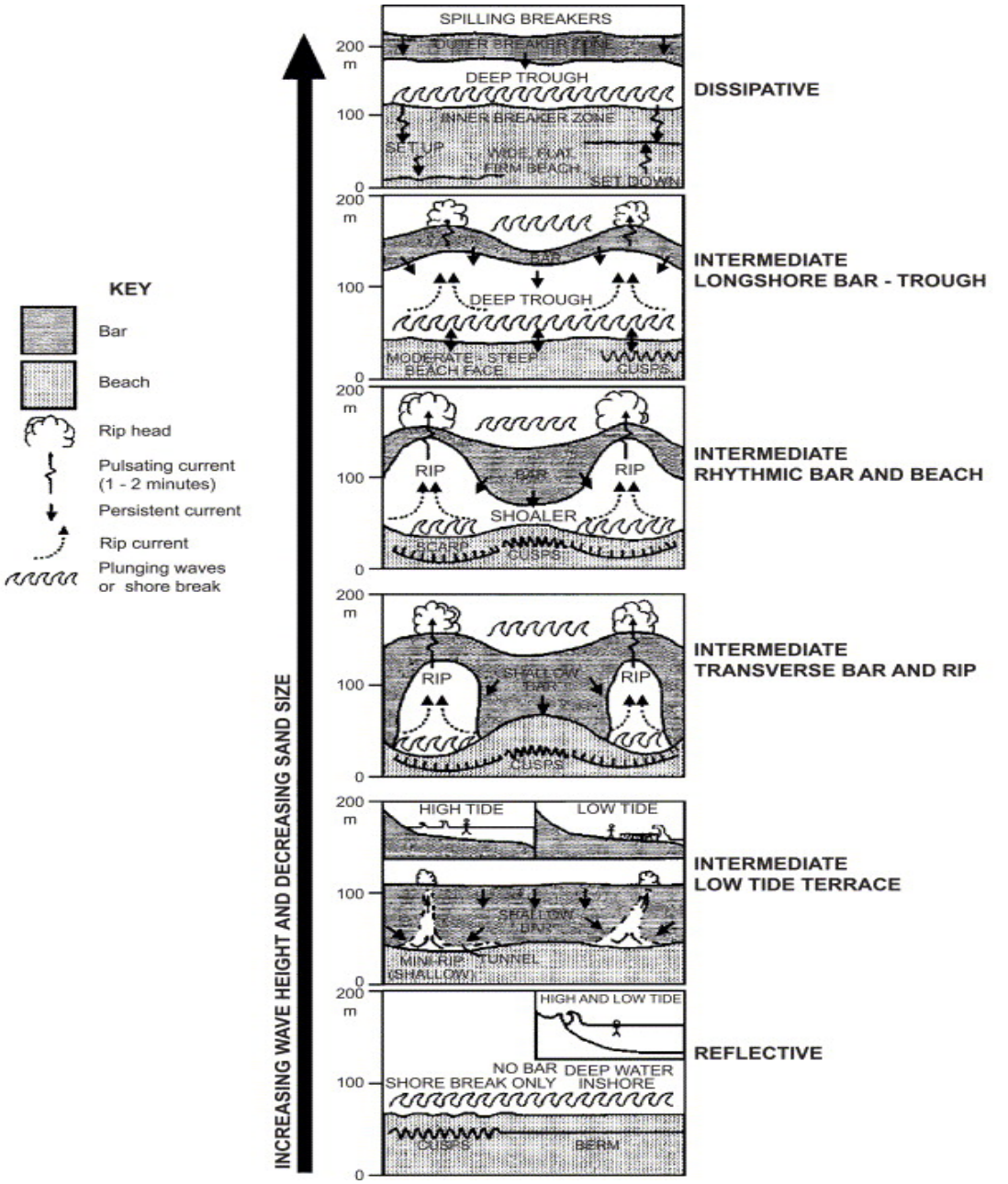

Figure 1. Classification scheme for beach morphology made by Wright and Short (1984)

intermediate states in the classification for single and double barred systems is to which level the pattern of the shoreline reflects the sandbar patterning (Wright and Short, 1984). A second element is to which extent the inner bar is attached to the shoreline (Price and Ruessink 2011).

2.1.3 Bar Coupling

The self-organization mechanism explains the morphology of both the inner and the outer bar individually. It has been observed in a double barred system that the alongshore spacing between horns and bays in the inner and outer bar frequently are equal. (Ruessink et al., 2007; Price and Ruessink, 2013). The matching patterns for the outer and inner bar indicate morphological coupling between the crescentic bars (Castelle et al, 2010a). Two types of morphological coupling occur, out of phase coupling and in phase coupling, which will be elaborated further below.

Out of phase coupling

Out of phase coupling occurs when a large fraction of the waves break over the crescentic outer bar. When waves propagate towards the outer bar, they initially break on the bay part of the outer bar. Due to this the set-up is stronger at the bay of the outer bar than its neighboring areas creating a gradient, that is not totally compensated by the radiation stress gradient, which results in a rip. Further shoreward the waves break on the horn of the outer bar resulting in a gradient in set-up, creating a current (Price and Ruessink, 2011; Price et al., 2013), see Figure 2a.

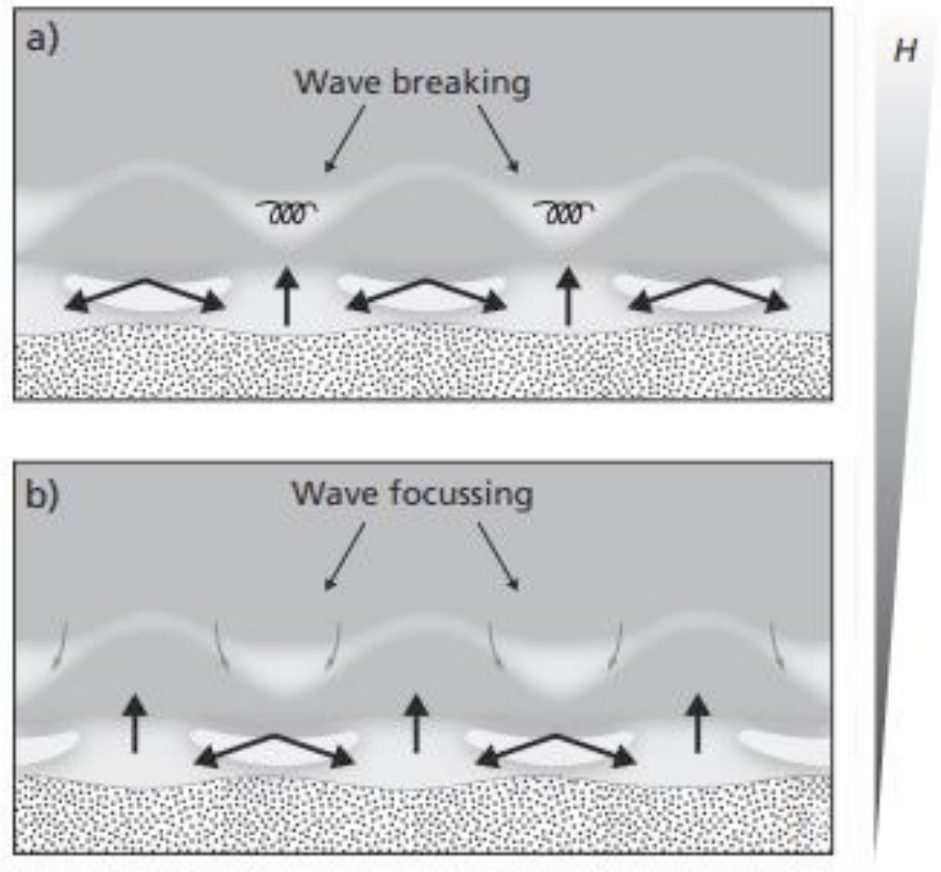

Figure 2 Coupling patterns derived by Castelle et al. (2010a) visualizing (a) out of phase coupling and (b) in phase coupling depending on energy conditions. Black arrows indicate flow patterns, while grey arrows indicate refractions patterns (Price et al., 2014).

In phase coupling

In phase coupling occurs during milder energetic conditions when the waves are not high enough to break on the outer bar. Nevertheless, the outer bar still influences the hydrodynamics conditions, resulting in shoaling and refraction. When the waves propagate towards the horn of the outer bar they refract causing the energy of the waves to be concentrated. As the waves propagate further towards the inner bar breaking occurs. Intense breaking occurs on the location with the concentrated energy, causing a gradient in setup, resulting in a rip (Price and Ruessink, 2011), see Figure 2b.

Three processes or parameters control the coupling between the sandbars and the shoreline and the extent to which it can occur (van de Lageweg, 2013). The first process is the variability of the water depth in the alongshore direction resulting in varying circulation patterns, causing the different coupling patterns (Price et al., 2014; Ruessink et al., 2007; Van de Lageweg, 2013). The second parameter is the cross-shore distance between the inner and the outer bar. The distance between the bars determines to what extent the sandbars can interact and thus couple. The third process is the angle of wave incidence, which can cause variations in the down- or up state sequence. With a downstate sequence including more alongshore variability, which causes a higher degree of coupling (Price et al., 2013; Price et al., 2014).

2.2 SPAWs

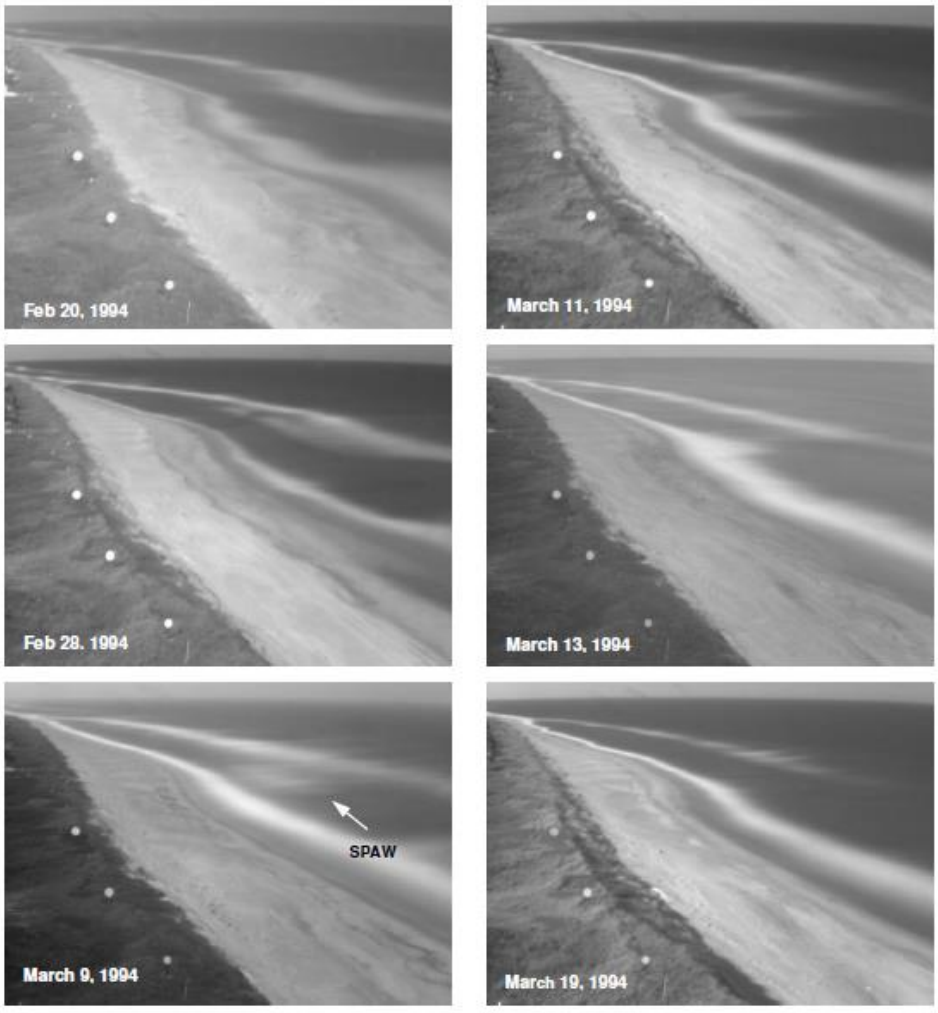

Figure 3 Sequence of time-exposure images near Duck (USA), exemplifying a SPAW-event (Wijnberg & Holman, 2007).

2.2.1 Definition

SPAWs were already described by Greenwood and Davidson-Arnott (1975), Konicki and Holman (2000) and Shand (2007), before being documented and named by Wijnberg and Holman (2007). Wijnberg and Holman (2007) defined a SPAW as a small bar-like feature that has shed from the shoreward side of a sandbar and subsequently migrates through the trough as an intact feature and eventually merges with the beach. Wijnberg and Holman (2007) called it a wave due to its similarities with a solitary wave in fluid dynamics. The similarities are that they both are isolated features that maintain their shape during the propagation and both have net displacement in the direction of the propagation. A SPAW can also migrate in a multiple bar system from an outer bar to a more shoreward (inner) bar (Almar et al., 2010; Price et al., 2017).

2.2.2 Initiation

The lifecycle of a SPAW can be divided in three phases: the formation, the migration and finally the welding with the beach/sandbar. The starting point of a SPAW is defined by Wijnberg and Holman (2007) as the moment when the SPAW separates from the bar. The exact mechanism leading to a formation of a SPAW is still poorly understood. However, observations have shown that the formation appears to be associated with the 3D bar pattern and high energetic wave conditions (Almar et al., 2010; Price et al., 2017). Throughout a storm the bar pattern is straightened (Van Enckevort et al., 2004). When a bar has a crescentic pattern the most shoreward part of the horn can separate from the sandbar and become a SPAW (Wijnberg and Holman, 2007; Almar et al., 2010; De Wit, 2017; Price et al., 2017; Korteling, 2017). Besides detaching from a horn, a SPAW can originate due to a bar bifurcation (Shand, 2007; Price et al., 2017; Korteling, 2017). The formation of a SPAW due to the separation of a bar bifurcation does not necessarily have to coincide with a crescentic pattern of the sandbars, as can be seen in Figure 4.

2.2.3 Migration

Once a SPAW is isolated from the sandbar it propagates through the trough to the beach or an inner sandbar. The duration of a SPAW event differs significantly, for instance at Duck (USA) the average duration was 17 days, with a minimum and maximum of respectively one week and seven weeks and a standard deviation of 9 days (Wijnberg and Holman, 2007). Furthermore, the duration varies per location with an average duration of approximately 40 days at Egmond (the Netherlands) (Price et al., 2017) and 9 days at the Surfers Paradise (Australia) (Korteling, 2017). The variation of the duration may lie in the distance between the bars and beach, or the size of the SPAW or bars, although this dependence is yet to be studied.
There is quite some uncertainty about the conditions that are favorable for the onshore migration of a SPAW. During the SPAW event that was studied by De Wit (2017) no movement was documented under low energetic conditions, while high energetic conditions coincided with the onshore migration of the SPAW to the inner bar. At Truc Vert (France) the opposite behavior was documented: during high energetic conditions the position of the SPAW remained nearly constant, while low energetic conditions resulted in a landward propagation to the inner bar (Almar et al., 2010). It has been observed that during the period of the migration a SPAW can erode and fail to merge with the inner sandbar or beach. At Egmond, it was found that this occurred predominantly during the winter months, which coincides with higher energetic conditions with obliquely incident waves (Price et al., 2017).

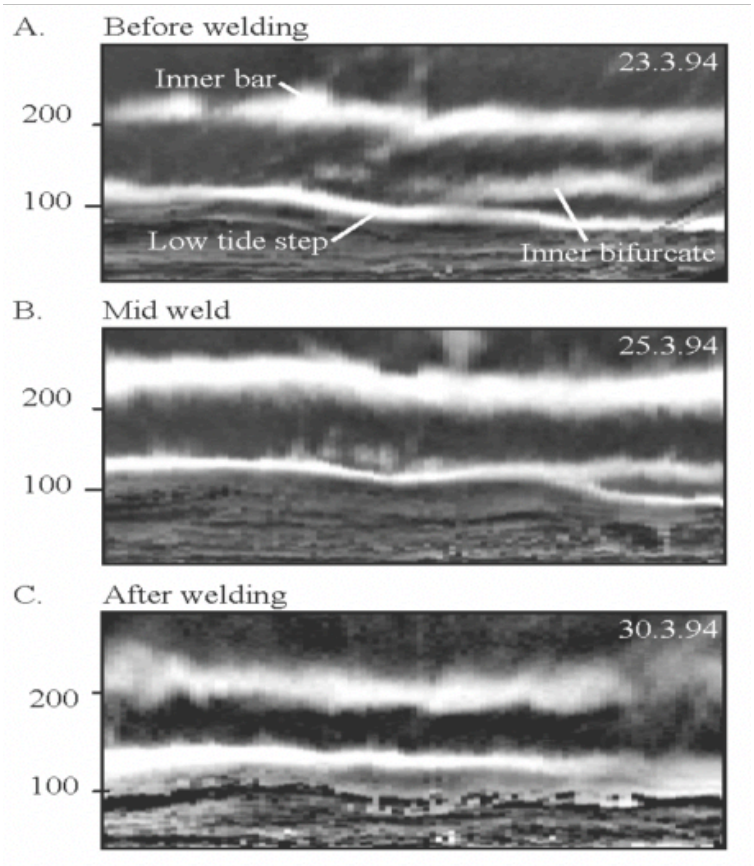

Figure 4 Example of an origination of a SPAW due to the separation of a bar bifurcation by means of rectified images depicting an inner bifurcate (A) incrementally welding to the inter- tidal beach (B and C) (Shand, 2007).

2.2.4 Shape, frequency and lifetime

The size of observed SPAWs differs widely between locations. Where the average length was approximately 130 metres at the location in Duck (Wijnberg & Holman, 2007), it was roughly 200 metres at the coast of Truc Vert Beach and Egmond aan Zee (Almar et al., 2010; Price et al., 2017). In both cases, however, the width was circa 30 metres, see Table 1. An estimation of the volume of a SPAW has been made in multiple studies. At the Duck coast a rough approximation had been made, which concluded the volume was 1900 m^3, assuming that the SPAW had an average height of 0.5m(Wijnberg & Holman, 2007). The volume of a SPAW at Truc Vert Beach was roughly estimated to be around 30000 m^3 (Almar et al., 2010). At the coast of Egmond aan Zee the volume has been estimated by means of an assimilation model that can estimate the bathymetry from a sequence of video images. With this model the volume of a SPAW at the coast of Egmond aan Zee was estimated to be 14700 m^3 (Price et al., 2017). Another SPAW at Egmond aan Zee has been observed, which had an average volume of 11000 m^3 by using the same model. The initial volume was approximately 7500 m^3, which accreted to 15800 m^3 when it welded with the shoreline. However, calculating the same SPAW event by time-exposure imaging the volume was estimated at 6000 m^3, indicating the difficulty of estimating the volume of a relatively dynamic SPAW by means of data assimilation.

Additionally, the frequency of a SPAW-event differs as well per location. Where at the Duck coast an average of 2 occurrences in a year were witnessed (Wijnberg & Holman, 2007), more than 6 events per year were observed at the coast of Egmond aan Zee (Price et al., 2017) and 7.8 events per year at the Gold Coast (Korteling, 2017). At Le Truc Vert Beach the duration time of the research was not sufficient to provide an annual frequency, it only stated that one event occurred during a research time of 5 weeks.

The differences between the SPAWs at the locations can be partly explained by the variances of the coasts. For example, the difference in frequency can possibly be explained by the sand budget of the coasts and the presence of a middle bar. If a middle bar is present, SPAWs can emerge from two bars. It can separate from the middle bar and weld to the inner bar or it can be separated from the inner bar and migrate to the shoreline. The variations between the transit time could result from the alternations in the dimensions of the SPAW and therefore the amount of volume. As large sand bodies react slower to wave conditions, which enlarges the transit time. Furthermore, the distance between the sandbars alters the transit times, both processes can be a partial explanation for the difference in transit time.

Table 1 Summary of conditions and SPAW characteristics at four different beaches (Ruessink et al., 2000[1]; Van Kuik, 2016[2]; Howd and Birkemeijer, 1987[3]; Wijnberg and Holman, 2007[4]; Almar et al., 2010[5]; Castelle et al., 2015[6]; Price and Ruessink, 2011[7]; Korteling, 2017[9]).

	Egmond aan Zee	Duck	Le Truc Vert	Gold Coast
Environment	Wave[1]	Swell[3]	Swell[5]	Swell[7]
Bar system	Triple[1]	Single/Double[3]	Double[5]	Double[7]
Slope	1:30[1]	1:12.5[3]	1:20[5]	1:50[7]
H_{rms} [m]	1.2[1]	1.0[3]	1.4[5]	0.8[7]
Tide [m]	1.3-1.6[1]	1-1.3[3]	1.5-4.5[5]	1.5-2[7]
Observed SPAWs	57[2]	19	1	47[8]
SPAW length [m]	218[2]	126 +/- 60[4]	100:250[6]	-
SPAW width [m]	30[2]	30 +/- 10[4]	72[6]	-
SPAW height [m]	-	Mean 0.5[4]	Mean 0.7; Max 1.0[6]	-
Transit time [days]	39[2]	17[4]	1[6]	9[8]
Frequency	6.7 per year[2]	1.95 per year[4]	1 in 5 weeks[6]	7.8 per year[8]
SPAW Volume [m^3]	14700	1900	30000	-

2.2.5 Dynamics

To determine the dynamics of a SPAW and the driving hydrodynamics, a modelling study was performed by Van der Weerd (2012). A base case was established with a schematized bathymetry to resemble a SPAW at Duck. A low wave height (H_s=0.56 m; T_p=8.2 s) was chosen with an average water level (z=0 m). Due to wave breaking over the SPAW and the coinciding dissipation of energy, wave heights differed spatially. These variations in wave height caused a cross-shore and alongshore gradients in radiation stress, leading to local set-up or set-down. The imbalance between radiation stress gradients and pressure gradients, namely residual forcing (Castelle et al., 2006; Bruneau et al., 2011; Castelle et al., 2012; Bouvier et al., 2019), indicates the net forcing available to drive nearshore currents. This resulted in the mean circulation field shown in Figure 5c, with dominant circulation at the edges of the SPAW and onshore directed flow above the SPAW. Due to the fact that the flow field was changed by the presence of the SPAW the sediment transport was altered correspondingly. The presence of the SPAW forced the waves to become more skewed and asymmetric, resulting in an onshore sediment transport over the SPAW. As can be seen in Figure 5b, on the shoreward side of the SPAW accretion took place while on the seaward side the SPAW eroded. During the low wave conditions of the base case the onshore sediment transport due to wave deformation was dominant over the onshore sediment transport due to the horizontal circulation current. In the modeling study of Van de Weerd (2012) multiple variables were altered in comparison the base case. A simulation with a reduced water level resulted in a higher wave set-up. Consequently, the pressure gradients are larger causing a stronger horizontal circulation current. The difference in sediment transport between both cases was however minimal.

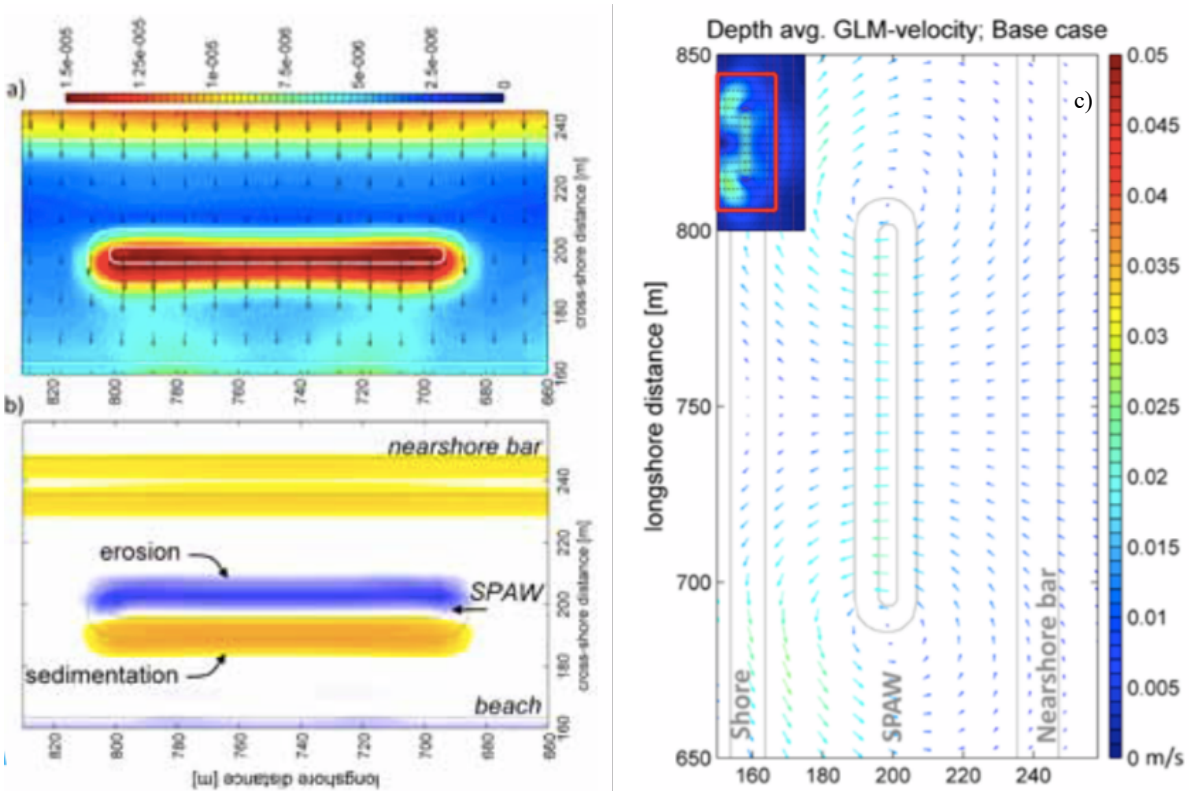

Figure 5 Top view of total load transport across SPAW (m3/m/s), (b) Top view of resulting initial sedimentation-erosion pattern across SPAW, (c) Top view of depth-averaged Generalized Lagrangian Mean velocity pattern around the SPAW location. Vectors show directions and magnitude, contour lines show bottom contours (Van der Weerd, 2012).5

The second variable that was altered was the cross-shore position of the SPAW between the bar and beach. This resulted in a stronger horizontal circulation current when the SPAW was near the bar and a weaker horizontal circulation current when the SPAW was closer to the beach. This caused a change in sediment transport. For the simulation where the SPAW was located near the beach the sediment transport was primarily concentrated around the tips of the SPAW. While the sediment transport was increased on the crest for the simulation where the SPAW was located closer to the bar.

Thereafter, the dimensions of the SPAW were altered, with a simulation for a longer SPAW and one with a wider SPAW. This resulted in a stronger horizontal circulation current for the wider SPAW and a more focused horizontal circulation current around the tips for the longer SPAW. Both cases had no considerable changes in sediment transport patterns.

The last simulation was run with a locally lower bar on the seaward side of the SPAW. This altered the depth average velocities with respect to the base case and were mainly directed through the depression in the lowered bar. The sediment transport increased at the locations where the bar had its original height. Furthermore, the flow pattern around the SPAW changed, the flow at the tips was slightly in the direction of the center of the SPAW, which was a result of a horizontal circulation current just landward of the SPAW. This could be an explanation for the SPAW maintain its shape during the propagation to the coast (Van der Weerd, 2012). In the study performed by Van der Weerd (2012) they were only able to simulate the initial timestep and therefor it remains unknown how the hydrodynamics and sediment transport processes will evolve during the onshore migration over time.

2.3 Research Question

Based on the performed literature study it is clear that there is much uncertainty about the onshore migration of SPAWs. Which processes are dominant in the onshore migration and which wave conditions or initial SPAW-geometry are favourable? What impact does a SPAW have to the nearshore morphology? Furthermore, what role does the angle of wave incidence play? As a hypothesis for the variation of the duration of the migration time could be the fact that the distance between the bars or bar and beach differs per location. It is the aim of this thesis to identify which processes are dominant in the morphodynamics of the migration of a SPAW, and how the presence of a SPAW impacts the nearshore morphodynamics. To reach this aim, the research is divided in the following questions and sub questions. The main question is: Which processes dominate the morphodynamics of the onshore migration of a SPAW? To resolve this subject the subsequent sub questions are formulated.

Onshore migration processes:

- What processes dominate the onshore migration of a SPAW during low energetic conditions?
- What is the role of wave-non-linearity (skewness and asymmetry) during the onshore migration of a SPAW?
- What is the role of circulatory currents during the onshore migration of a SPAW?

Wave characteristics:

- How does the angle of wave incidence affect the onshore migration of a SPAW?

SPAW initial morphology:

- How does the width of a SPAW influence the onshore migration?
- How does the cross-shore position of the SPAW influence the onshore migration?

SPAW impact on nearshore morphodynamic:

- What impact does the presence of a SPAW have on the nearshore morphology?
- How does the presence of a SPAW influence the alongshore variability?

3. Study site & methods

3.1 Study Site

For the boundary conditions underlying this model study we used Egmond aan Zee, where SPAWs have been observed to migrate from the outer to the inner bar regularly (Price et al 2017). At Egmond aan Zee an average of 6 SPAW events are witnessed annualy, with an average dimension of 200m x 30m. Egmond aan Zee is located in the central part of the Dutch coast, see Figure 6. The coast at Egmond aan Zee is characterised as a microtidal wave-dominated coast, with a tidal range varying from 1.2 meters at neap tide to 2.1 meters at spring tide. The tidal currents are asymmetric with a dominant component towards the North (Giardano et al., 2010). The coast has a typical offshore wave height of approximately 1 - 1.5 meters, with periods of 4-5 seconds. The dominant wave directions are from the northwest and southwest. The coastal profile is characterised as a three-bar system and has a roughly 50m wide beach backed by a dune system. The outer bar is located approximately 500 meters offshore and its crest is around -3 m below MSL (Mean Sea Level). The outer bar and inner bar are separated by a through which has a depth of around -5 m below MSL. The inner bar is located 200m offshore and its crest as a height of approximately -1 m below MSL. Between the inner bar and the swash bar there is a through with a depth of around -2 m below MSL. The cross-shore slope is roughly 1:100 (Van Duin et al., 2004).
At Egmond aan Zee the sandbars experience net offshore migration (Ruessink and Kroon, 1994) with a period of about 15 years (Wijnberg, 2002). During this process the alongshore-averaged distance between the sandbars tend to double. The temporal variations in alongshore variability of the sandbar decreases in the seaward direction, with wavelengths of respectively 30-100 for the swash bar and 1000-3000m in the inner and outerbars. The location is generally characterised by medium well-sorted sands (0.25 – 0.5 mm), in the trough between the inner and outer bar the sand is moderately sorted and coarser (> 0.5 mm) (Elias et al., 2000).

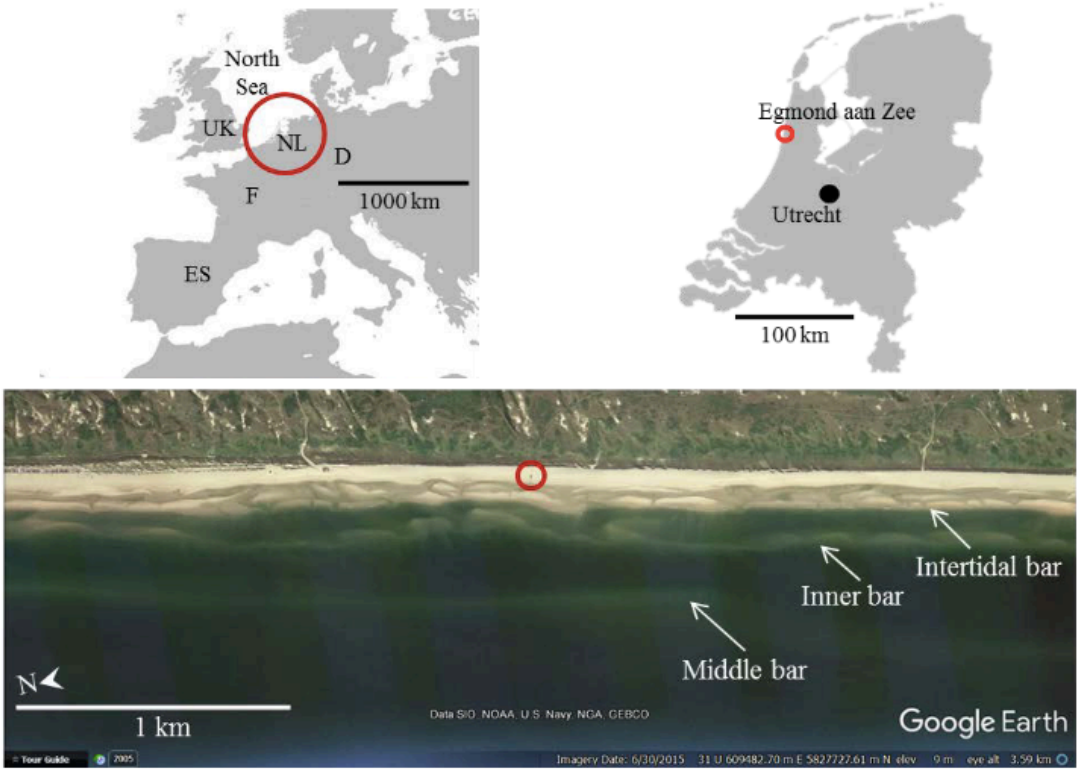

Figure 6 Location of Egmond aan Zee in Europe and the Netherlands (top), and the typical beach morphology (below) (Price, 2017).

3.2 Numerical morphodynamic model

The model that was used is a nonlinear morphodynamic model 2Dbeach, (Dubarbier et al., 2017 ; Bouvier et al., 2019) on which the cross-shore sediment transport processes from (Dubarbier et al., 2015) have been implemented. By doing this, the basic state assumptions from the version of (Castelle et al., 2012) were removed. The model consists of four combined modules: a spectral wave model, a shortwave-averaged and depth-integrated flow model, an energetic-type sediment transport model, and a bed evolution model.

3.2.1 Wave module

The statistical wave fields are computed from the spectral wave model SWAN (41.10 version) (Booij et al., 1999). The dissipation model proposed by (Battjes and Janssen, 1978) was used, with a constant breaker parameter $\gamma = 0.73$ (Battjes and Stive, 1985). For the intrawave motion, the model acquires a parametrization of the wave-skewness that relates values of wave-skewness and asymmetry to the local Ursell number, which are derived from field measurements of the statistical wave field and mean water level (Ruessink et al., 2012).

3.2.2 Circulation module

The circulation module was based on the depth- and phase-averaged nonlinear shallow water equations, assuming balance of momentum and conservation of water mass, which, using the Einstein substitution reads:

$$\frac{\partial Q_i}{\partial t} + \frac{\partial}{\partial x_j}\left(\frac{Q_i Q_j}{h}\right) + gh\frac{\partial \eta}{\partial x_j} + \frac{1}{\rho}\frac{\partial S_{ij}}{\partial x_j} - \frac{1}{\rho}\frac{\partial T_{ij}}{\partial x_j} + \frac{\Gamma_i^b}{\rho} = 0$$

$$\frac{\partial \eta}{\partial t} + \frac{\partial Q_j}{\partial x_j} = 0$$

where h is the mean water depth, $Q_i = hU_i$ are the water volume fluxes, where subscript *i* is refers to the two horizontal coordinates (x and y). The depth-averaged velocity is U_i (Mei et al., 1989), S_{ij} is the radiation stress tensor, Γ_i^b is the bed shear stress tensor (Phillips, 1977), η is the mean surface elevation, g is the gravitational acceleration, ρ is water density and T_{ij} is the lateral mixing term that describes the horizontal momentum exchange due to the combination of breaking induced turbulence and the mean current. Bed return flow was computed according to the wave radiation stress formulation by Phillips (1977), assuming a depth uniform vertical distribution. The morphological time step is selected to be notably shorter than the variations of offshore wave conditions, but longer than the infragravity timescale.

3.2.3 Sediment transport module

The total sediment transport Q_t is computed with an energetics-type transport model composed of three modes of transport, which is based Hsu et al. (2006), Dubarbier et al. (2015), Dubarbier et al. (2017), Bouvier et al. (2019) and Rutten et al. (2019, as

$$\vec{Q}_t = \vec{Q}_w + \vec{Q}_c - \vec{Q}_g$$

with transports related to wave velocity skewness $\vec{Q}_w$, wave induced mean current $\vec{Q}_c$ and downslope gravitational effect $\vec{Q}_g$, which prevents unrealistic bar growth and unstable bar shapes. Furthermore, $\vec{Q}_w$ accounts for the wave nonlinearity but disregards the contribution of wave asymmetry and swash motion. These three modes of transport correspond to the 2-D extension of the formulations which are further explained in Dubarbier et al. (2015) and are defined as:

$$\vec{Q}_c = C_c \left[K_b < \left|\vec{U}(t)\right|^2 \left(\overline{u}_i + \overline{u}_j\right) > + K_s < \left|\vec{U}(t)\right|^3 \left(\overline{u}_i + \overline{u}_j\right) > \right]$$

$$\vec{Q}_w = C_w \left[K_b < \left|\vec{\tilde{u}}(t)\right|^2 \tilde{u}(t) \left(\frac{k_i + k_j}{\left|\vec{k}\right|}\right) > + K_s < \left|\vec{\tilde{u}}(t)\right|^3 \tilde{u}(t) \left(\frac{k_i + k_j}{\left|\vec{k}\right|}\right) > \right]$$

$$\vec{Q}_g = C_g \left[\frac{K_b}{\tan\phi} < \left|\vec{U}(t)\right|^3 > + \frac{K_s \varepsilon_s}{w_s} < \left|\vec{U}(t)\right|^5 > \right] \left(\partial_i Z_f + \partial_j Z_f\right)$$

Where subscript i (j) indicates the cross-shore (alongshore) component, ϕ = 32° the friction angle of sediment, k the wave number and w_s the sediment fall velocity. $K_b = \rho \frac{\varepsilon_b}{\tan\phi}$ and $K_s = \rho \frac{\varepsilon_s}{w_s}$ are coefficients linked to bed load and suspended load transport, ρ is the water density and ε_b and ε_s are two numerical coefficients according to Dubarbier et al. (2015). The total velocity field is divided in two components $\vec{U}(t) = \vec{\overline{u}} + \vec{\tilde{u}}(t)$, where $\vec{\overline{u}}$ is the time- and depth averaged mean flow and $\vec{\tilde{u}}(t)$ is the orbital velocity defined at the top of the bottom boundary layer. The contribution of the three individual transport components to $\vec{Q}_t$is scaled with free friction components C_c, C_w and C_g.
In the last module, bed level change was updated through the sediment mass conservation equation, which was looped back into the wave model. Running though the four modules, small perturbations in the bathymetry can grow and become self-organizing rhythmic patterns through positive feedback loops between the flow field and bed level.

3.3 Model set-up

A nested Cartesian grid was implemented during the modelling of this research. This fine grid consists of 85 grid cells in the alongshore direction with a cell width of 20m and 56 grid cells in the cross-shore direction with a cell width of 10m. Which combines to a total modelled area of 560 x 1700 m. For the wave module an extended grid (3 times in the alongshore direction) was used to avoid any 'shadow area' when modelling with oblique incoming waves. There is no vertical grid as the values for the currents and sediment transport are depth averaged. Furthermore, the nearshore waves and currents were computed on the fine grid using lateral periodic conditions for the circulation module.

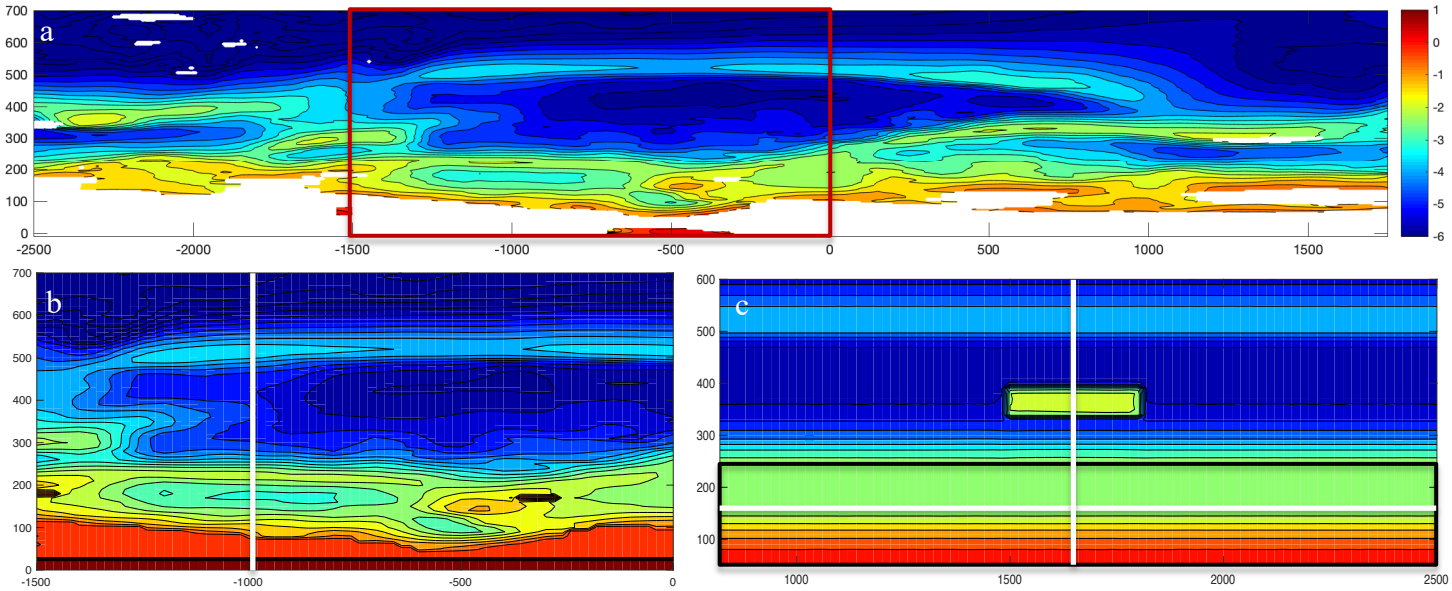

Figure 7 (a) Derived bathymetry from a bathymetric survey of the coast of Egmond aan Zee, with a red box for the extracted part. (b) extracted part of the bathymetric survey, with chosen profile of which the synthetic bathymetry is derived (white line) (c) synthetic bathymetry including chosen cross-shore and alongshore profiles as white lines and in black the extent of the nearshore zone.

The synthetic bathymetry is derived from a bathymetric survey of the coast of Egmond aan Zee at November 2019 (Figure 7a). From the measured bathymetry a section was extracted to get a usable sized area, see the red box (Figure 7a). In the extracted part a single cross-shore profile was chosen, see Figure 7b, which did not have the SPAW in it but had a relative shallow trough. This profile used for the creation of the synthetic grid by extending it uniformly along the coast. Resulting in an alongshore uniform, double-barred beach system, wherein a SPAW was placed (Figure 7c). An alongshore profile at X=160 m, a cross-shore profile at Y=1650 m and a defined nearshore zone were used in the analysis in this research, described below.

3.3.1 Inputs

The contribution of the three individual transport components to $\vec{Q}_t$ is scaled with free friction coefficients C_c, C_w and C_g which were kept as default settings (0.08, 0.08 and 0.24 respectively). These settings were parameterized to permit the simulation of a downstate sequence (Dubarbier, 2017). Additionally, ε_b and ε_s are two numerical friction coefficients which are respectively 0.135 and 0.15 according to Dubarbier et al. (2015). To avoid non-physical wave refraction at the SPAW extremities, limiters (l=0.05) were used for spectral wave propagation (Dietrich et al., 2013). Furthermore, C_f is a bottom friction coefficient which controls the flow intensity and has a value of 0.012. Mixing terms ν_0 and M that affect the shape and size of the horizontal circulation were kept at the same values as (Bouvier, 2019), which are 10 $m^2 \cdot s^{-1}$ and 5 respectively. The sediment transport was computed with a spatial consistent *d50* of 250µm, which is in range of the beach grainsize of Egmond aan Zee. The used morphological timestep is 1 hour.

3.3.2 Cases

In total, a number of 17 cases were defined for which the model was run. For the SPAW base case scenario, a SPAW was implemented with a width of 300 m, length of 50 m and a water depth of 2 m above the SPAW. These measurements were chosen based on the general dimensions of SPAWs which were observed in Egmond aan Zee (Section 3.1) and a measured SPAW at the coast from November 2019. Furthermore, the cross-shore location was 340-390 m and the alongshore location in the middle of the grid from 1500-

1800 m. For the wave action a wave height of 1.5m was chosen with a wave period of 8s and an angle of wave incidence of 15°, with a directional spreading of 20°. Tides were disregarded in this study. The same scenario was also established without a SPAW to see how it could affect the morphodynamics in the nearshore zone. For this simulation the same inputs for wave action were used, the only difference is the absence of the SPAW.

For the differing scenarios to the base different input values were varied, while some maintained the same value through all simulations. The height of the SPAW was consistent throughout all the simulations at -2 m below sea level just as the wave period at 8 seconds. The exact configurations can be seen in Table 2.

Table 2 Characteristics for all the simulations sorted by variables

	H_s (m)	T_p (s)	θ	Width (m)	Length (m)	Height (m)	Cross-shore location (m)
Base	1.5	8	15°	300	50	-2	340-390
No SPAW	1.5	8	15°	-	-		-
Lowered wave height	0.5	8	15°	300	50	-2	340-390
Cross-shore location	1.5	8	15°	300	50	-2	300-380 - 380-430
SPAW dimension	1.5	8	15°	100-500	50	-2	340-390
Higher angle of wave incidence	1.5	8	0-50°	300	50	-2	340-390

3.4 Analysis & Definitions

To quantity the increase of sediment to the shore a measurement of the volume of the nearshore zone was created. To create this measurement first the nearshore zone (not to be confused with the actual nearshore zone) had to be defined, which can be seen in Figure 7c in the black box: it ranged from 50-250 m cross-shore. To quantify the volume difference in this area a reference level of -5 m below water level was used, which was below any elevation encountered in the defined nearshore zone. The volume of the nearshore zone was defined as all the volume above this reference level in the defined nearshore zone.

A variable α was made in order to estimate the alongshore variability of the inner bar over time. The root mean square error (α) was computed of the elevation of the alongshore profile located at the cross-shore location x = 160m, which can be seen in Figure 7c as a white line. Wherein the mean elevation of the profile at each given timestep was used to compute variable α .

$$\alpha = \sqrt{\sum_{i=1}^{n} \frac{(Z_i - Z_{mean})^2}{n}}$$

The motion of the SPAWs were traced to visualise their migrationpath. This was done by setting their initial location in the middle of the SPAW and tracing the highest grid cell in the surrounding area. This surrounding area consisted of the 20 meters in both cross-shore directions and 100 meters in both alongshore directions, from the previous located highest point, which can be seen in Figure 8. By differing the alongshore search area similar findings were found, for the cross-shore direction however a wide search area resulted in skipping to the inner sandbar and not following the SPAW.

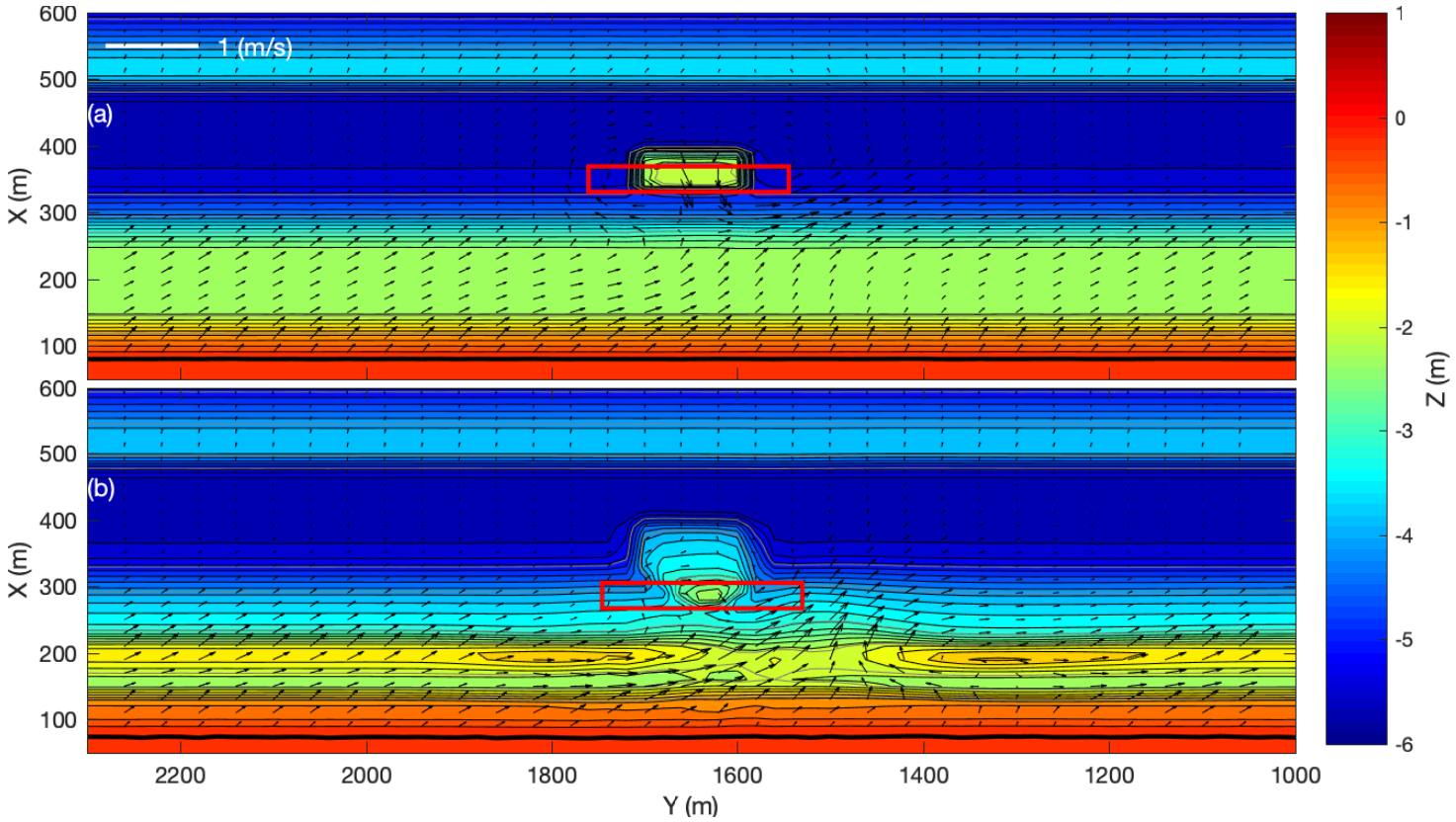

Figure 8 Top view of morphodynamic evolution of the coast and with the arrows indicating the modeled currents for a simulation at timestep a) 2 hours, b) 33 hours. The red boxes indicate the search area for the highest elevation for determining the migration path. The color bar shows the seabed elevation in meters and the dark line indicates the mean sea level shoreline.

4. Results

In this Chapter, the modelling results are presented, beginning with the no SPAW base case to see the influence of such a feature on sandbar dynamics. Thereafter the SPAW base case is elaborated and both base cases are compared for their evolution in alongshore variability and volume in the nearshore zone. Subsequently, the results of the simulated scenarios are presented, where three variables were explored: first the cross-shore start location, followed by the dimension of the SPAW and lastly the angle of wave incidence.

4.1 Base Cases

4.1.1 No SPAW Base Case

Figure 9 shows the morphodynamic evolution of the coast in a downstate sequence in six timesteps for the no SPAW base case. In Figure 9a and b the inner sandbar (first visible around x=200 m) gets more elevated, with the bar depth increasing from -2.1 m (a), through -1.3 m (c) to -0.3 m by the end of the simulation. In the next timestep the inner sandbar has migrated in the onshore direction and has increased further in elevation. The coast has no alongshore variability at this point in the simulation. In Figure 9d the inner sandbar has nearly welded with the shoreline and two elevated spots in the inner sandbar can be witnessed. At both sides of these locations an offshore-directed current is visible. An alongshore current is visible in the small trough between the inner sandbar and the shore according to wave incidence. In Figure 9d and e the formation of rips is visible, creating a periodic alongshore variability with rip channels.

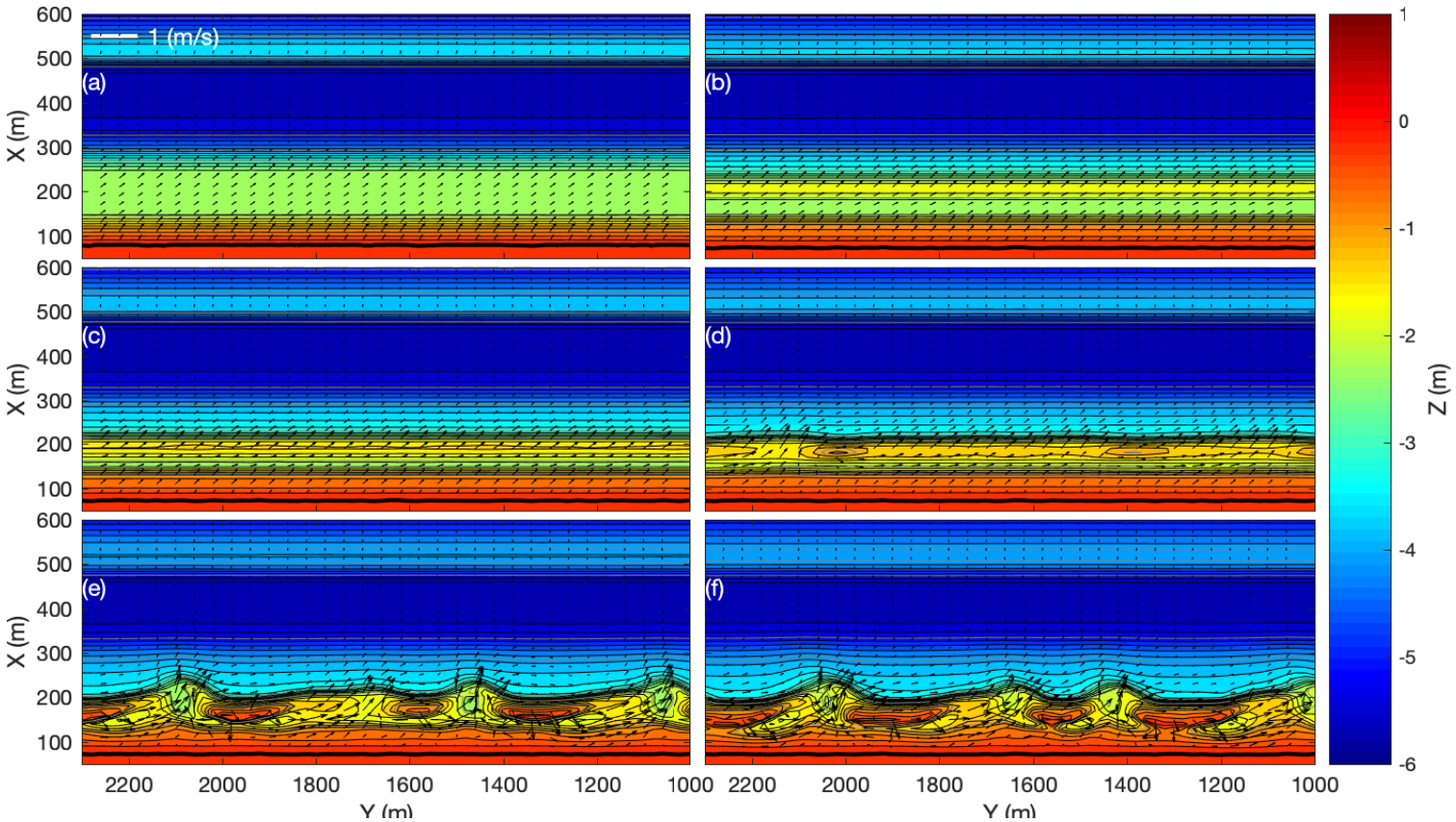

Figure 9 Top view of morphodynamic evolution of the coast and with the arrows indicating the modeled currents for no SPAW base case at timestep a) 2 hours b) 20 hours c) 40 hours d) 60 hours e) 80 hours and f) 100 hours. The wave forcing consists of a wave height of 1.5m, a wave period of 8s and an angle of wave incidence of 15°. The color bar shows the seabed elevation in meters and the dark line indicates the mean sea level shoreline.

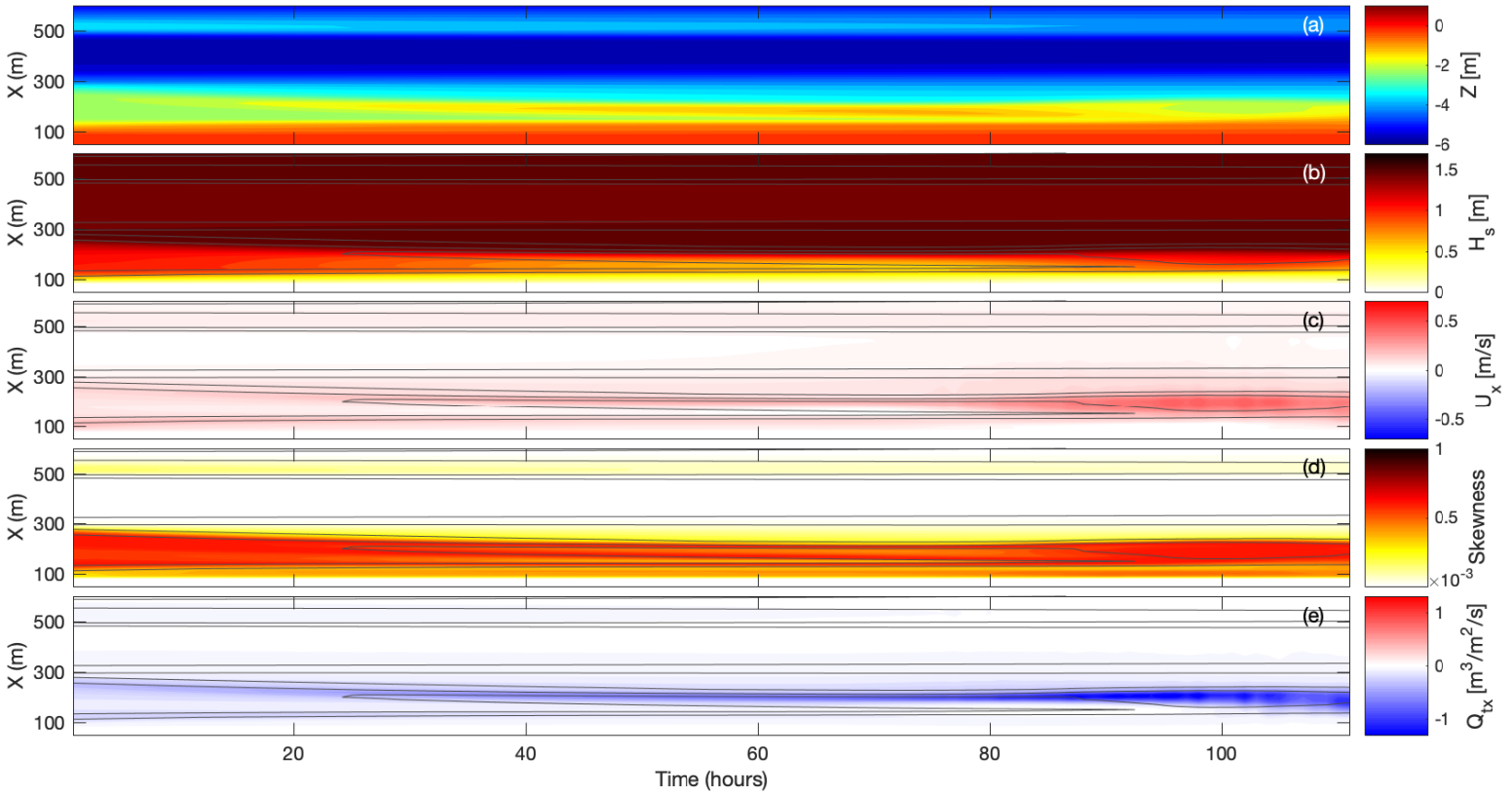

Figure 10 The evolution of the cross-shore profile at the alongshore location of 1650 over time for the no SPAW base case visualizing a) the elevation b) the wave height c) the current in the cross-shore direction d) skewness e) depth averaged sediment transport in the cross-shore direction.

Figure 10 shows the evolution of the cross-shore profile at the alongshore location of Y= 1650m, of the elevation, wave height, current in the cross-shore direction, skewness and sediment transport in the cross-shore direction over time for the no SPAW base case. When the outcomes of Figure 9 are compared to Figure 10 they have an astonishing resemblance. Whereas it can be seen in Figure 10a that the inner sandbar gradually welds to the shore. Subsequently, in Figure 10b the waves do not break over the outer sandbar and lose their main energy over the inner sandbar. This is in line with the outputs of Figure 10d which shows skewness on the inner sandbar alone. When looking at the cross-shore current and sediment transport in Figure 10c and e there is an offshore current and an onshore transport of sediment on the inner sandbar during the whole simulation. With an increased intensity of the current and transport at the end of the simulation this coincides with the arisen rip current in the cross-shore profile.

4.1.3 SPAW Base Case

It is generally visible that through time the SPAW migrates in the onshore direction. In the Figure 11a a circular current is visible on the tips of the SPAW with an onshore directed current on top of the SPAW and a seaward directed current next to the SPAW. This originates from an imbalance between the pressure gradients and radiation stress. At this stage the bathymetry is still alongshore uniform.

In Figure 11b the higher elevated area of the SPAW has migrated in the onshore direction, in a relatively alongshore uniform manner. Additionally, the inner sandbar has grown except at the alongshore location landward of the SPAW. The circular currents on the tips of the SPAW are still present. However, on the leeward side of the SPAW a rip current is beginning to form across the inner bar.

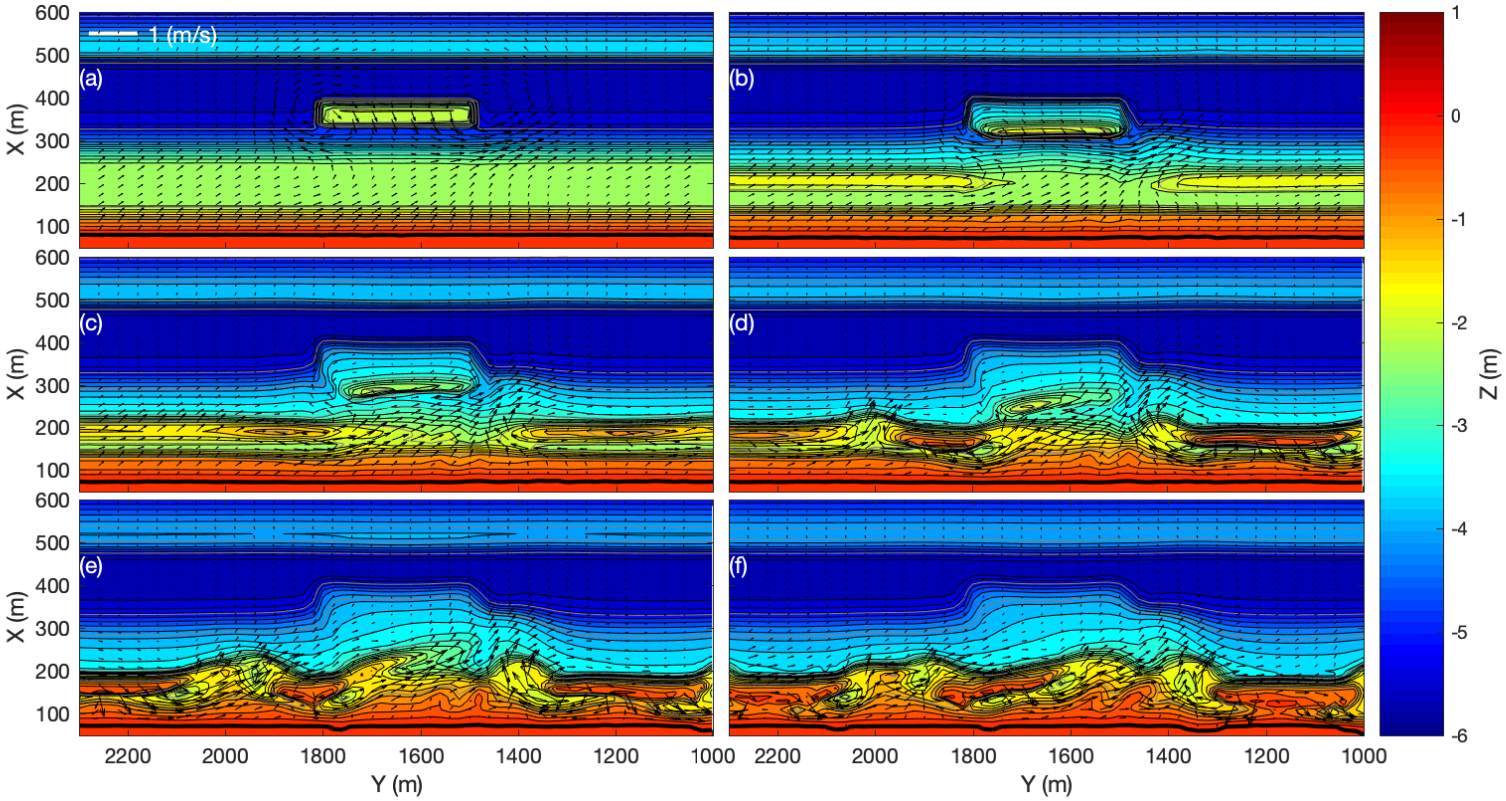

Figure 11 Top view of morphodynamic evolution of the coast and with the arrows indicating the modeled currents for the SPAW base case at timestep a) 2 hours b) 20 hours c) 40 hours d) 60 hours e) 80 hours and f) 100 hours. The wave forcing consists of a wave height of 1.5m, a wave period of 8s and an angle of wave incidence of 15°. The color bar shows the elevation in meters and the dark line indicates the mean sea level shoreline.

In Figure 11c the SPAW has migrated further onshore. It is now less elevated than in the previous timesteps and has left a trail of sand over the area it has migrated across. It can be seen, in Figure 11c, that the SPAW is no longer alongshore uniform, but that the most elevated part is now located at the left side of the SPAW. Furthermore, the left side of the SPAW has migrated further onshore than the right side. Also, in the inner sandbar some alongshore variability has started to develop in the higher elevated areas landward of the SPAW and higher elevated areas adjacent to the alongshore boundaries of the SPAW. The observed current across the inner bar at the leeward side of the SPAW in Figure 11b has increased in magnitude and reaches further seaward than the rip currents from the no SPAW base case. The circular pattern has disappeared at the right side of the SPAW, whereas it is still present at the left side of the SPAW.

In Figure 11d the SPAW has migrated further onshore, although it is predominantly the left side of the SPAW that has migrated. The dimension of the SPAW and its elevation is fairly similar as in Figure 11c. It is visible that the trail that the SPAW leaves has a boundary perpendicular to the shoreline on the right side and more at an angle at the left side. At the alongshore location of 2000 and 1400 m rips start to form, where the rip located at 1400 converges with the previous observed seaward directed current on the leeward side of the SPAW. It is visible that the inner bar as whole has migrated onshore and has merged with the beach landward of the SPAW. At the same time, the elevated areas in the inner sandbar, indicated in Figure 11c, grew substantially. The observed current at the leeward side of the SPAW in Figure 11c has increased in magnitude and the circular current is no longer observed.

In Figure 11f the SPAW attaches with the left side to the inner bar and while the attached part of the SPAW becomes more elevated than in Figure 11e, the right side seems to have lost sediment over time. The inner bar has merged with the beach and takes a more crescentic shape with bays at the locations of the rips. At the same time, the right

boundary of the trail on top of the seaward directed current, an increase in sediment forms a rip head. In Figure 11f the SPAW is completely merged with the inner bar and has become a more elevated part of it. The rip at Y = 2000m has filled up, while the rip at Y = 1400m is still active and flows together with the current located at the leeward side of the remnants of the SPAW.

Figure 12 shows the evolution of the cross-shore profile at the alongshore location of Y= 1650m, of the elevation, wave height, current in the cross-shore direction, skewness and sediment transport in the cross-shore direction over time for the SPAW base case. Figure 12a shows the onshore migration of the SPAW, including the trail of sand over the area it has migrated across. When this is compared to the wave height in Figure 12b, it can be seen that during the whole simulation the initial wave breaking occurs on the SPAW and does not occur on the trail or outer sandbar. The remaining wave breaks on the inner sandbar and shore. This is supported by Figure 12d where the skewness is visualised. In Figure 12c there is an onshore directed current over the SPAW and an offshore directed undertow at the shoreline. While the onshore directed current over the SPAW fades away at approximately 40 hours an onshore directed current returns at the shoreline at 90 hours. For the sediment transport an onshore directed transport is visible over the SPAW during the complete simulation as well as the inner sandbar. The transport intensifies during the moments that the SPAW welds to the inner sandbar. To further analyse the sediment transport processes involved in the onshore migration of the SPAW, the individual sediment transport components in the model are analysed below.

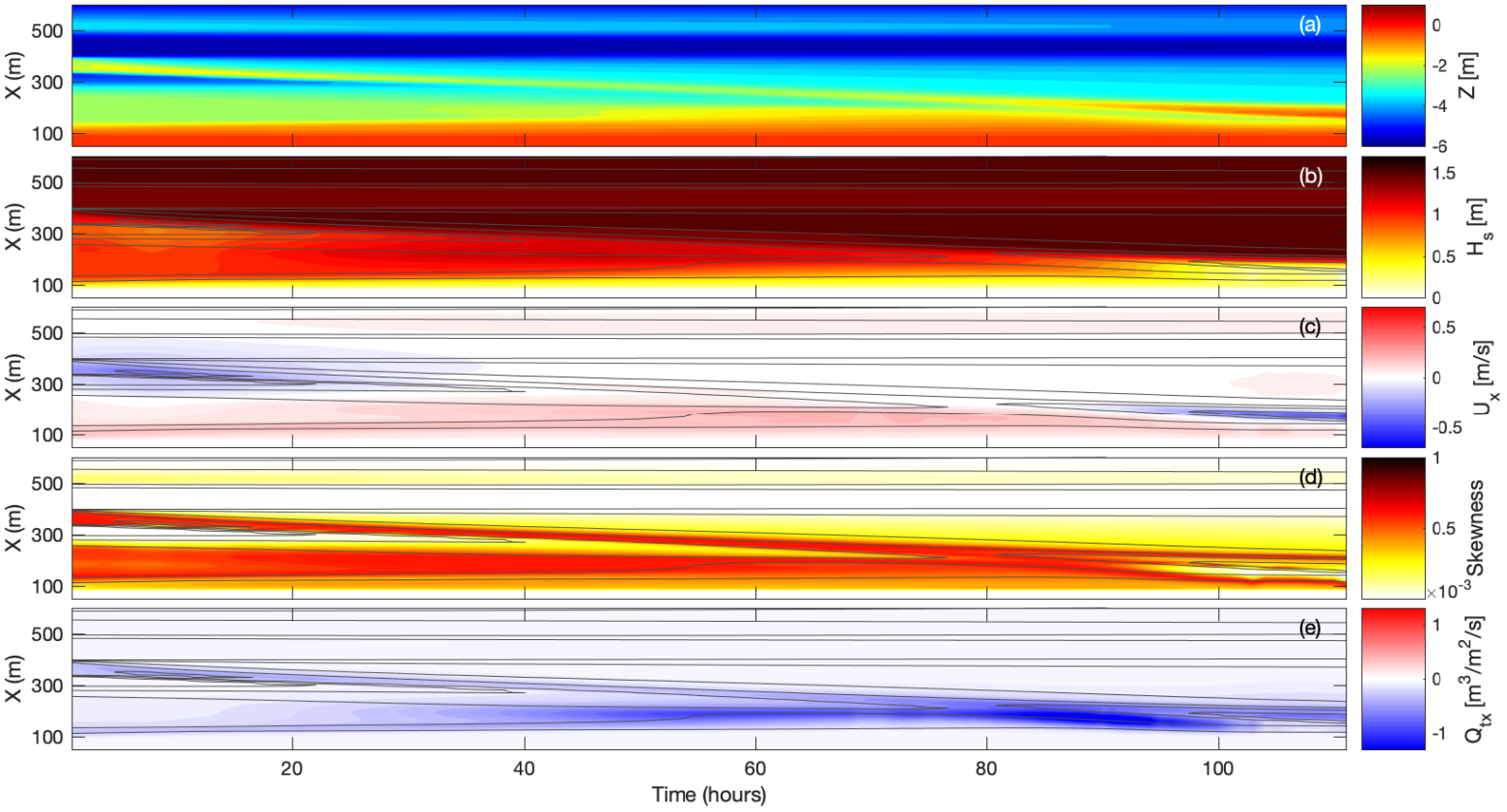

Figure 12 The evolution of the cross-shore profile at the alongshore location of 1650 over time for the SPAW base case visualizing a) the elevation b) the wave height c) the current in the cross-shore direction d) skewness e) depth averaged sediment transport in the cross-shore direction.

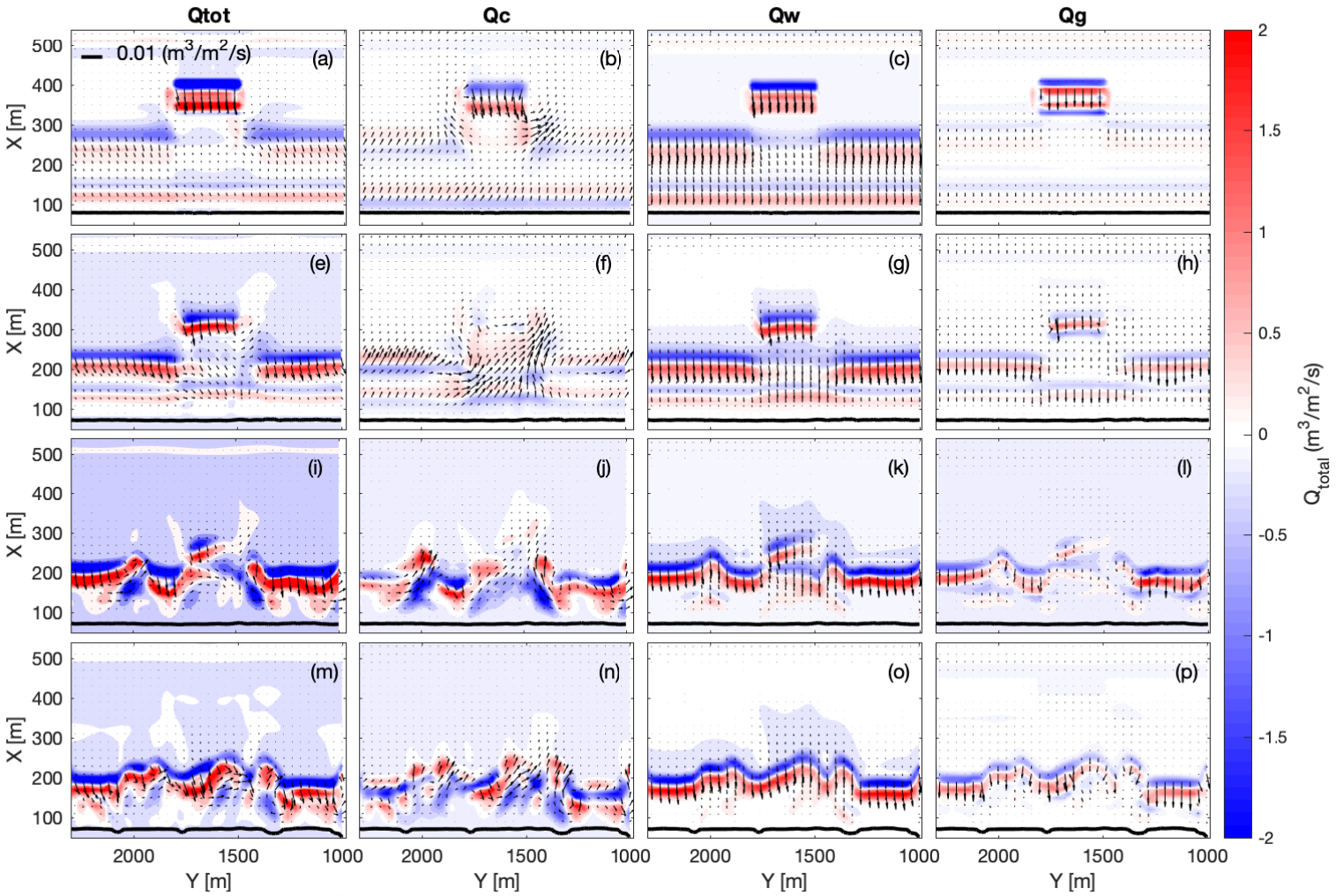

Figure 13 Erosion/accretion patterns for the SPAW base case driven by the total sediment transport (first column) and the sediment transport due to currents (second column), wave action (third column), and the gravitational component (fourth column), with the arrows indicating the sediment fluxes. The first row (a-d) at 2 hours, second row (e-h) at 33 hours, the third tow (i-l) at 67 hours and the last row (m-p) at 100 hours. The colorbar shows the vertical change in seabed elevation in [m3/m2/s] and the dark line indicates the mean sea level shoreline.

Figure 13 shows the erosion and accretion patterns due to currents, wave action, gravitational component and combined together for the SPAW bas case for four different timesteps. It can be observed that in the first timestep for all the components there is an onshore directed transport of the SPAW. Where for the wave action component there is an additional onshore directed transport over the inner bar. For the current driven component there is minor offshore directed transport at this location. With respect to the currents the gravitational component and the wave action component merely result in an onshore directed component over the SPAW, while the current driven component shows besides the onshore directed current over the SPAW the initiation of the rip current and circular currents at the tips of the SPAW.
In the second timestep the gravitational and current component have relatively small values contributing to the onshore migration of the SPAW. While the current driven component shows large sediment fluxes related to the circulation around the SPAW. Furthermore, the current component shows minimal accumulation or erosion around the SPAW, while the wave action component clearly visualises the onshore directed transport of the SPAW and inner sandbar. Due to the low values of the gravitational and current components the total sediment transport has a high similarity with the wave action component for this timestep. For the current driven component an offshore directed transport is visible for the inner sandbar, while the rip current is visible just as the circular current at the left side of the SPAW.

In the third timestep it is visible that only the gravitational component has relatively low values. The wave action component shows an onshore migration of a smaller SPAW area than in the previous timestep. At the same time, the SPAW experienced a counterclockwise rotation. For the current driven component, no evolution around the SPAW is witnessed and has areas of elevation increase and decrease around at the horns and bays of the inner sandbar. No circular currents are present, while the rip at the leeward side of the SPAW can still be witnessed. This gives the total sediment transport at the third timestep a combination of onshore transport due to the waves action component and local accretion or erosion in the vicinity of the inner bar due to the current component. In the last timestep the SPAW has welded to the beach therefor only action around the inner sandbar is visible in Figure 13. Whereas the wave action component continues to provide an onshore directed transport and the current component creating rips.

4.1.3 Alongshore variability

Figure 14 shows the evolution of the alongshore profile located at 160m cross-shore distance through time for the base case with and without SPAW. It can be observed in Figure 14 that without a SPAW a relatively regular crescentic pattern forms with respect to the formation of the rips. The spacing between the rips is between 100 and 200 meters and for all the rips the formation begins around 65 hours. The first alongshore variability coincides with the formation of the rips. Where the currents have are onshore directed on the elevated areas while the currents are offshore in the rips. Furthermore, it is visible that the rips migrate substantially to the leeward side, with respect to the angle of wave incidence with time. When the evolution of the alongshore profile is compared with the SPAW base case it is clearly visible that the first alteration occurs sooner around timestep 40 for the SPAW base case at the alongshore location of the SPAW. This coincides with the first measured alongshore variability. The gradual welding of the

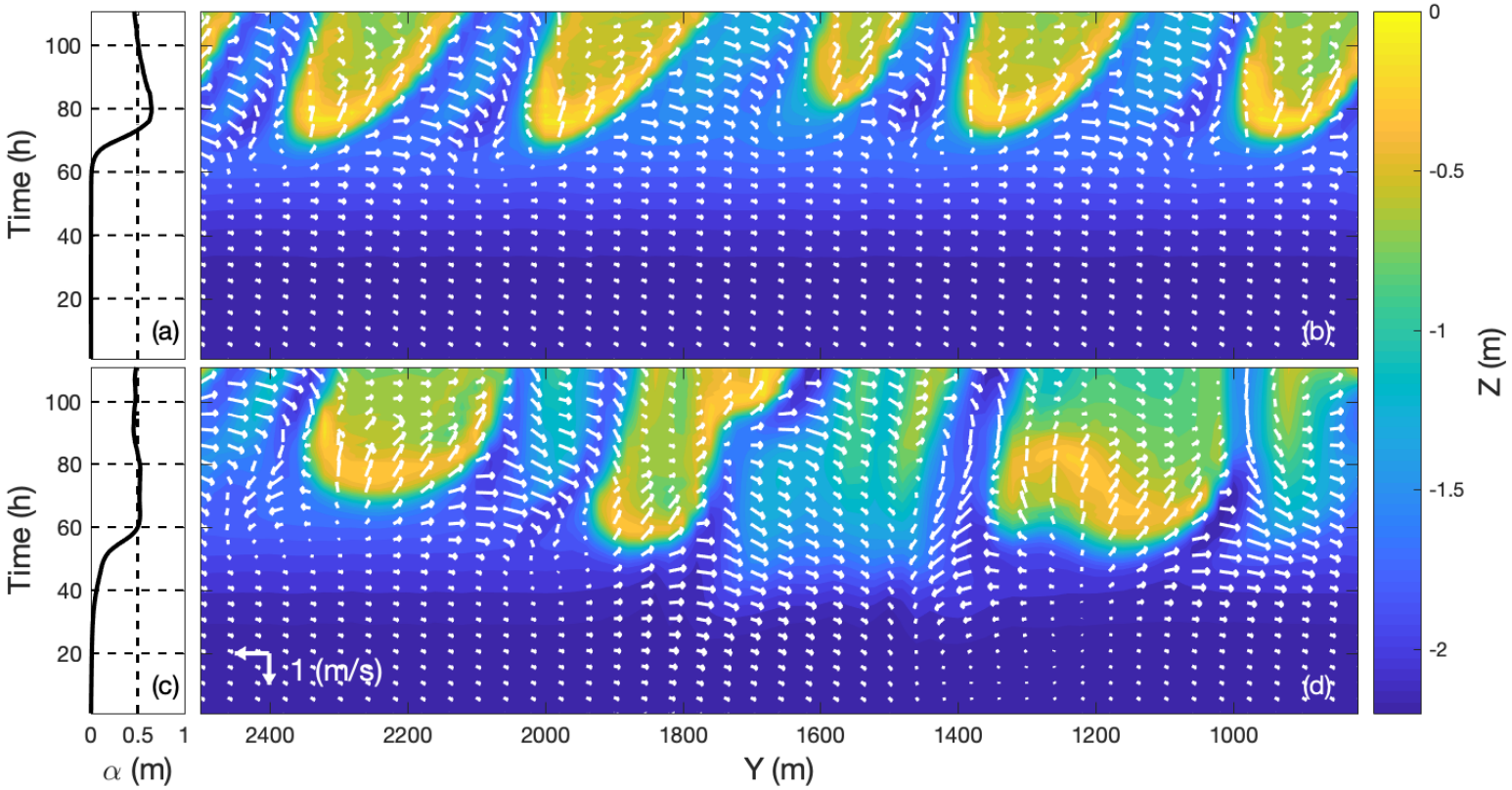

Figure 14 The evolution of the alongshore profile and the alongshore variability at 160m cross-shore distance through time, with the arrows indicating the modeled currents, for no SPAW base case (a-b) and the SPAW base case (c-d). The colorbar indicates the elevation in meters. Arrows indicating currents, with arrows facing the bottom denoting an offshore directed current.

SPAW is visible, just as the narrowing of the SPAW through time. Additionally, the rip pattern is less consistent, with a lower number of elevated areas, which are generally wider. For the SPAW base case the rips migrate to a lesser extent to the leeward side. At the same time of the welding on both sides of the SPAW an obliquely offshore directed current is visible. The currents of the SPAW base case are slightly stronger than for the no SPAW base case

The root mean square error of an alongshore profile, at cross-shore distance of X= 160m, acts as measure for the alongshore variability, as the cross-shore dimension is disregarded. Figure 14a shows that for no SPAW base case the first increase in alongshore variability is measured at about 60 hours, thereafter the RMSE rises steeply to 0.65, after which it gradually decreases to a value of 0.5. When this is compared to the base case including a SPAW, Figure 14c, the first alongshore variability is seen around 20 hours where after it gradually increases until timestep of 50 hours to a value of 0.2. After that moment it rapidly increases to 0.5 where it continues to stay relatively consistent for the rest of the simulation. And so, both simulations end with a similar alongshore variability, while this value was reached at an earlier stage for the no SPAW base case. For the SPAW base case the peak was higher but occurred at a later stage.

4.1.4 Volume of the nearshore zone

Figure 15 shows the evolution of the volume of the defined nearshore zone (50-250m in the cross-direction) over time for the SPAW base case and the no SPAW base case. The no SPAW base case increases rapidly in the beginning of the simulation. This initial rapid increase coincides with the onshore migration of the inner bar in the defined nearshore zone. Thereafter it is relatively stable for a long time in the end a small decrease is visible. For the SPAW base case a slightly less rapid increase is visible, and the volume stabilizes at a lower point. At approximately 50 hours the volume starts to increase gradually, which coincides with the SPAW entering the defined nearshore area. This increase continues to the end of the simulation.

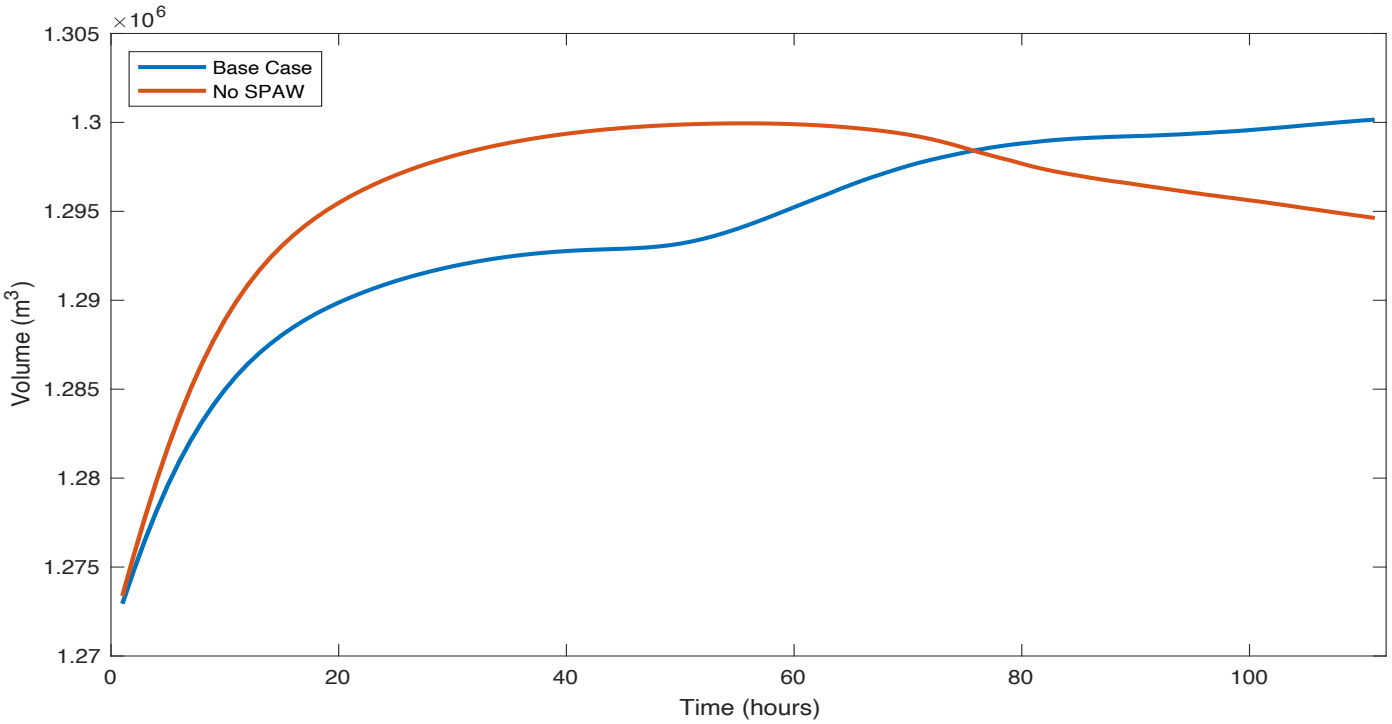

Figure 15 The evolution of the volume of the nearshore zone through time, for no SPAW base case and SPAW base case.

4.2 Cross-shore location SPAW

Multiple simulations were executed with a wide variety of cross-shore starting locations. In this Chapter two of those simulations are discussed in detail, with a cross-shore starting location 20 m further onshore and 20 m further offshore, respectively.

4.2.1 Morphodynamics of further onshore located SPAW

Figure 16 shows the morphodynamic evolution of the coast in six timesteps for a simulation with a SPAW located at X= 320-370m, 20m further onshore than the base case. The initial timestep looks very similar to the one in Figure 11, next to the fact that the SPAW is located further onshore and the circular current on the edges of the SPAW is only present on the updrift side of the SPAW. In the second timestep a similar process occurs, with respect to the SPAW base case, the inner sandbar gets more elevated and the current on the leeward side of the SPAW originates, flowing in the seaward direction. On the updrift side of the SPAW a second rip current originates as in the SPAW base case with a lower magnitude and which is oriented perpendicular to the leeward rip current. In Figure 16c it is visible that the SPAW has migrated further in the onshore direction and that the SPAW has not rotated. The SPAWs dimensions are fairly similar to Figure 16b, which differs from the SPAW base case. Although the length seems to have decreased a small amount. The morphologic development of the inner bar is very similar with the SPAW base case. The currents on the leeward and updrift side of the SPAW are still present, as is the circular current at the updrift edge of the SPAW. Additionally, the trail the SPAW leaves has a more oblique boundary at the updrift side were the rip

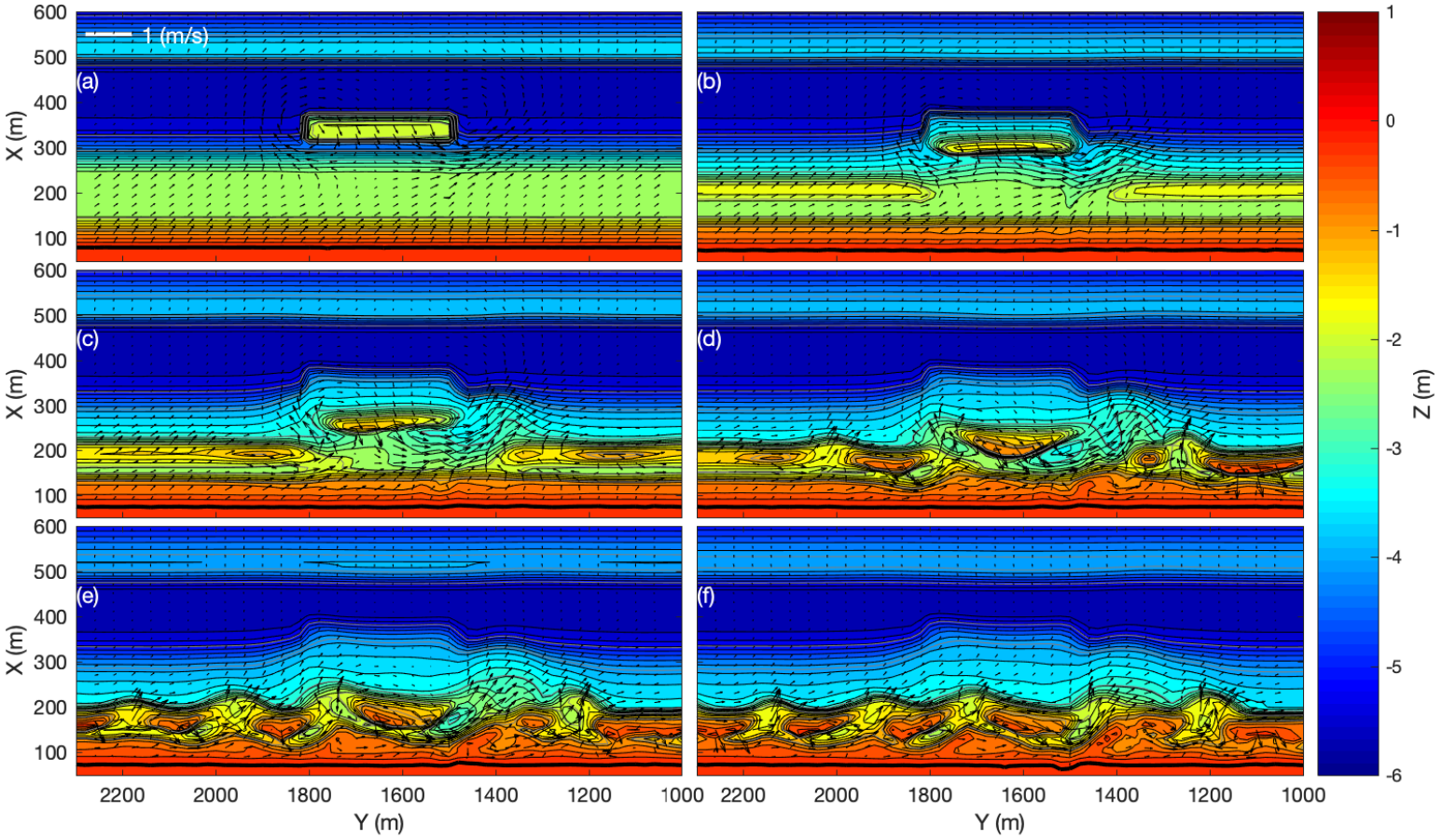

Figure 16 Top view of morphodynamic evolution of the coast and with the arrows indicating the modeled currents with the start position of the SPAW located 20 meters further onshore, at timestep a) 2 hours b) 20 hours c) 40 hours d) 60 hours e) 80 hours and f) 100 hours. The wave forcing consists of a wave height of 1.5m, a wave period of 8s and an angle of wave incidence of 15°. The color bar shows the seabed elevation in meters and the dark line

current is present. The bulge witnessed were the leeward rip current flows in the seaward direction in Figure 11c is present at the same location. At the next timestep (Figure 16d) it can be observed that the SPAW has taken a V-shape and is more elevated than in the previous timestep, which is not observed in the SPAW base case.

The circular currents at the edges of the SPAW are absent, while the rip currents between the SPAW and the inner sandbar have increased in intensity. In Figure 16e and f the SPAW has welded with the inner sandbar and the flow velocities in the rip currents reduce as the rips fill in. While this takes place for the updrift rip current in Figure 16e, it occurs in Figure 16f for the leeward rip current.

4.2.2 Morphodynamics of further offshore located SPAW

Figure 17 shows the morphodynamic evolution of the coast in six timesteps for a simulation with a SPAW located 20m further offshore. In the first two timesteps (Figure 17a and b) a similar image is visible with respect to the SPAW base case in Figure 11. Although, it can be seen in Figure 17b that the elevation gap in the inner sandbar is smaller than for the SPAW base case. The circular currents at the tips of the SPAW are present in both the first timesteps and the rip current on the leeward side of the SPAW is present from Figure 17b. At the next timestep the SPAW has decreased in elevation substantially and begins to form a trail with a straight boundary at the leeward side of the SPAW and an oblique boundary at the updrift side. The circular currents at the tips of the SPAW are not visible anymore. The intensity of the rip current at the leeward side of

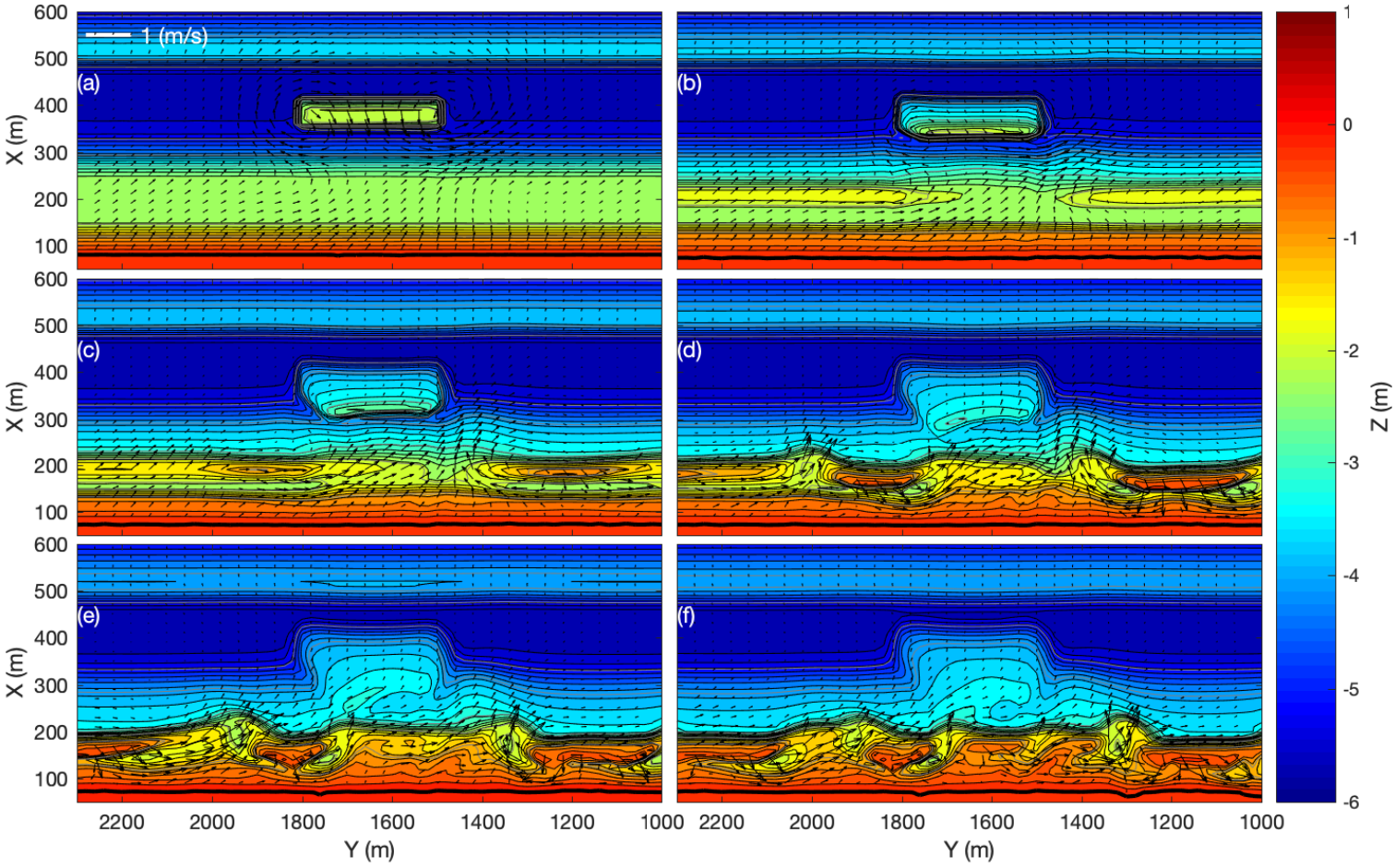

Figure 17 Top view of morphodynamic evolution of the coast and with the arrows indicating the modeled currents with the start position of the SPAW located 20 meters further offshore, at timestep a) 2 hours b) 20 hours c) 40 hours d) 60 hours e) 80 hours and f) 100 hours. The wave forcing consists of a wave height of 1.5m, a wave period of 8s and an angle of wave incidence of 15°. The color bar shows the seabed elevation in meters and the dark line indicates the mean sea level shoreline.

the SPAW has increased. In Figure 17d the SPAW has lost elevation over time. At the same time, it rotated in the counterclockwise direction to a similar extent as in the base case. The rip current at the leeward side of the SPAW remains present. At 80 hours the SPAW has only a small elevation difference with the trail of sand it has migrated across, which is approximately -3.5 meters. The remnants of the SPAW have almost welded to the inner sandbar and rotated further in a counterclockwise direction. Furthermore, the rip current at the leeward side of the SPAW has decreased in intensity. In Figure 17f the SPAW is no longer visible and what was left of it has welded to the coast. The trail of sand that has been left behind has migrated onshore although clearly not in the same rate as the SPAW. Additionally, the rip current at the leeward side of the SPAW cannot be observed anymore.

4.2.3 Volume of the nearshore zone

Figure 18 shows the evolution of the volume of the nearshore zone through time, for simulation with variations the initial cross-shore location. Initially no clear relation is visible in Figure 18 between the cross-shore start location and the amount of volume in the nearshore zone. However, some relations can be found when the figure is studied in detail.
The steep volume increase at the beginning of the simulation is less intense for the SPAWs which have a cross-shore start position located closer to the coast.
Where the least increase in the beginning of the simulation is for the SPAW in the most shoreward located position.
However, it is for these cases which have a more shoreward located starting position that after a short moment of no change the volume increases for a second time, which coincides with the SPAW entering the defined nearshore zone. This increase is strong when it begins, however it flattens over time but increasing till the end.
While for the cases which have a more seaward located starting position the initial increase, coinciding with the onshore migration of the inner sandbar, continues for a

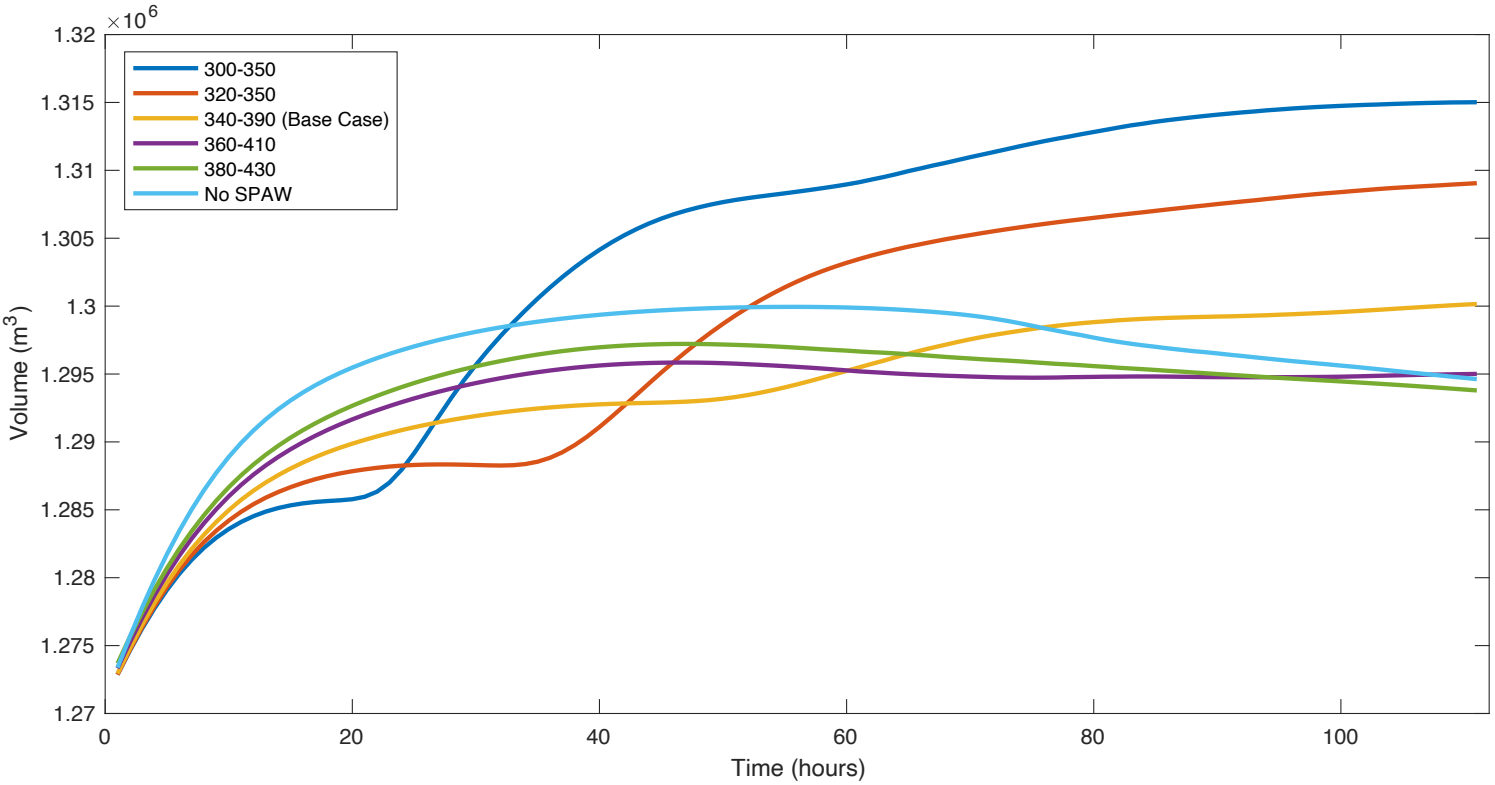

Figure 18 The evolution of the volume of the nearshore zone through time, for the simulations varying the cross-shore start location of the SPAW and the no SPAW base case.

longer time period. Hereafter the volume is relatively stable and does not decrease to same extent as the no SPAW base case.
So, in general a more shoreward located starting position results in a larger volume entering the defined nearshore zone over time, while it also results in a smaller initial increase in the beginning of the simulation. For the further seaward located SPAWs the length of the simulation was not long enough to see the total effect of the SPAW.

4.3 SPAW dimension

Six simulations were executed with a wide variety of SPAW dimensions. In this Chapter of those simulation two extremes are discussed in detail, with a SPAW with a width of 100m and 500m.

4.3.1 Morphodynamics of a smaller SPAW

In Figure 19 the migration of a SPAW with the width of 100m can be seen. Whereas Figure 19a is similar to the SPAW base case from Figure 11a, with the exception of the dimension of the SPAW. This includes the presence of the circular currents at the tips of the SPAW. Further on in Figure 19b the SPAW has migrated in the onshore direction and a relatively small gap in the elevation of the inner sandbar is observed. Subsequently, the circular currents at the tip of the SPAW are no longer visible. The rip current at the leeward side of the SPAW has initiated. In the Figure 19c the size of the SPAW has decreased substantially and that the SPAW has migrated further in the onshore direction with respect to the SPAW base case in Figure 11c. At the same time the SPAW has gotten a spherical shape. The rip current at the leeward side of the SPAW has increased in

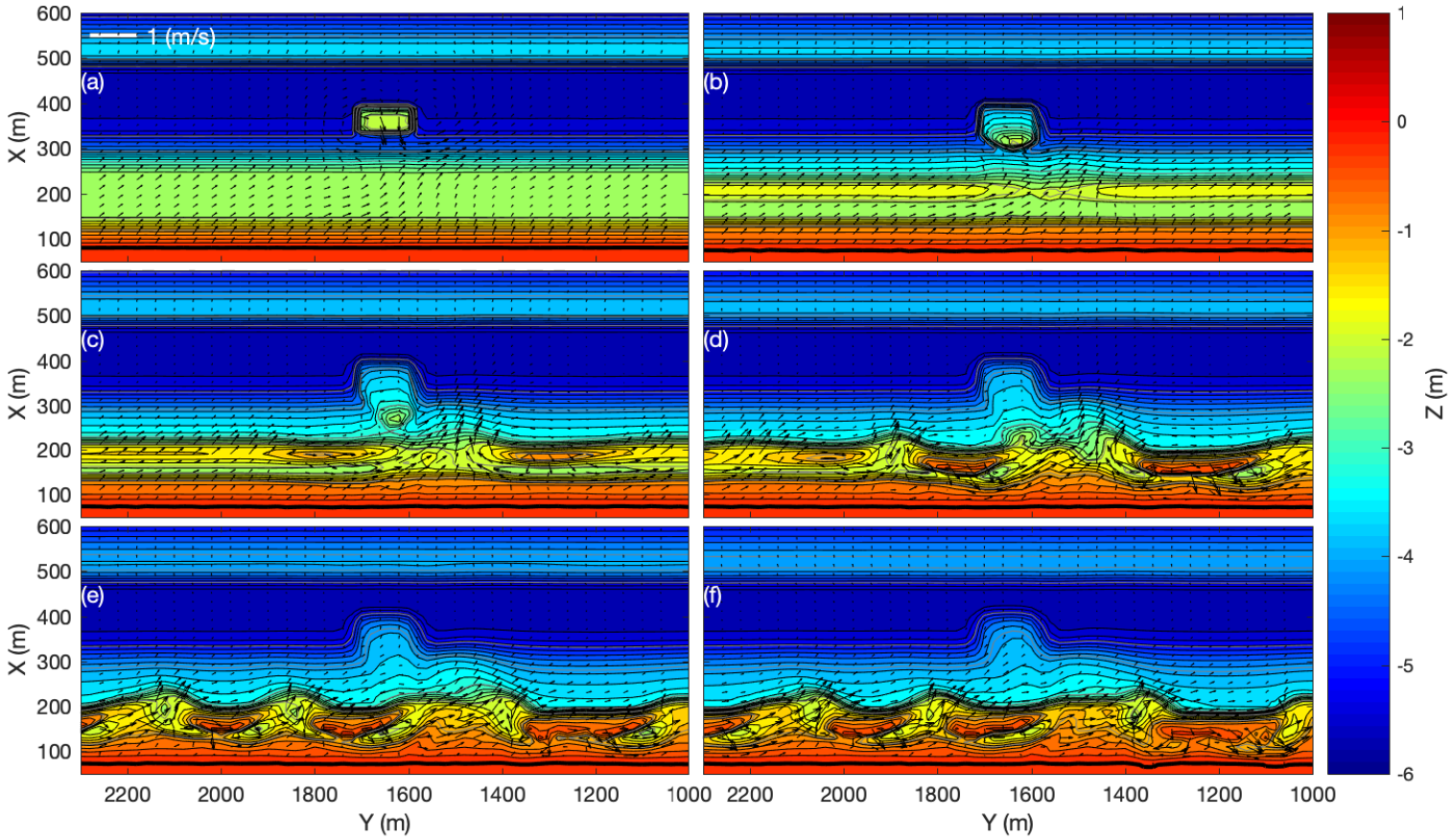

Figure 19 Top view of morphodynamic evolution of the coast and with the arrows indicating the modeled currents for a SPAW with a width of 100 meters, at timestep a) 2 hours b) 20 hours c) 40 hours d) 60 hours e) 80 hours and f) 100 hours. The wave forcing consists of a wave height of 1.5m, a wave period of 8s and an angle of wave incidence of 15°. The color bar shows the seabed elevation in meters and the dark line indicates the mean sea level shoreline.

intensity. In the next timestep the SPAW has welded to the inner sandbar, while the welding in the SPAW base case occurred a timestep later.
Furthermore, the rip current that was present at the leeward side of the SPAW is still present at the same location. The trail of the SPAW looks relatively perpendicular to the coast at the leeward boundary, while the updrift boundary is obliquely oriented. This results in a narrowing trail in the onshore direction. In Figure 19e and f remnants of the trail of the SPAW remain to be transported in the onshore direction. The rip current that was present on the leeward side of the SPAW decreases in intensity and migrates as a whole more in a leeward direction.

4.3.2 Morphodynamics of a wider SPAW

In Figure 20 the migration of a SPAW with the width of 500m is visualised. In the initial timestep the circular currents at the tips of the SPAW are present. In the next timestep the SPAW has migrated in the onshore direction and has created an elevation gap in the inner sandbar of approximately the size of the SPAW. Rip currents on both sides of the SPAW are present and the circular currents at the tips of both sides of the SPAW are still present as well however with a decreased intensity. In Figure 20c it can be seen the SPAW has decreased in elevation. Additionally, the rip currents at both sides of the SPAW are still present. The rip current at the leeward side has increased in intensity, while this is not the case for the rip current at the updrift side of the SPAW. The elevation gap in the inner sandbar is still present, however on the updrift side of the gap sediment has been deposited. The updrift tip of the SPAW has been tilted to a small extent in the onshore direction, while the rest of the SPAW has been parallel to the coast. In the next timestep the SPAW has lost elevation, especially at the leeward side. The rip current at the updrift side of the SPAW has vanished, while the rip current at the leeward side has

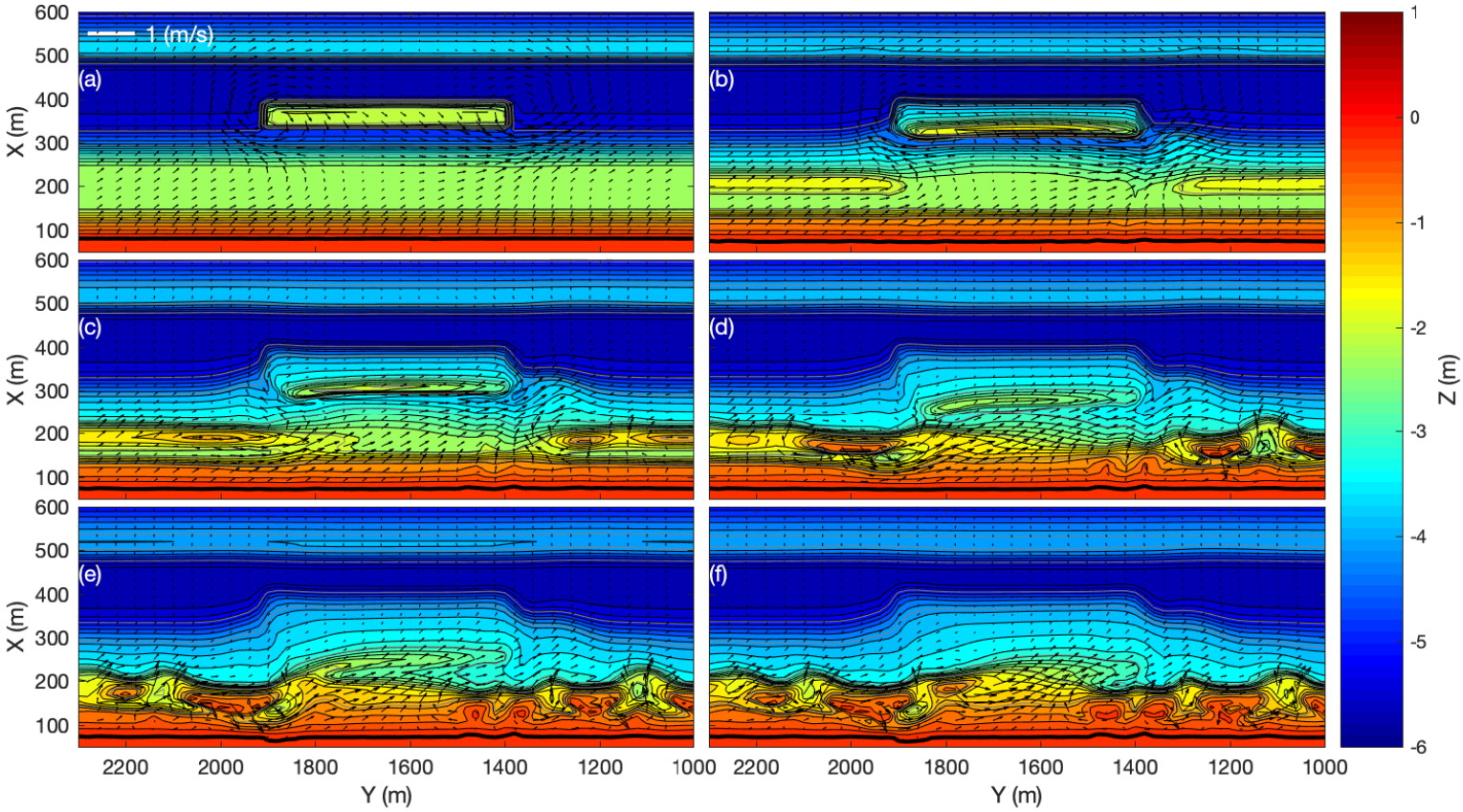

Figure 20 Top view of morphodynamic evolution of the coast and with the arrows indicating the modeled currents for a SPAW with a width of 500 meters, at timestep a) 2 hours b) 20 hours c) 40 hours d) 60 hours e) 80 hours and f) 100 hours. The wave forcing consists of a wave height of 1.5m, a wave period of 8s and an angle of wave incidence of 15°. The color bar shows the seabed elevation in meters and the dark line indicates the mean sea level shoreline.

decreased in intensity. In Figure 20d the updrift side of the SPAW has tilted in the onshore direction, while this was only the tip in the previous timestep. The leeward side of the SPAW remains parallel to the shoreline. In Figure 20e the already tilted updrift side of the SPAW now has merged with the inner sandbar, which on its own has connected with the shoreline. The updrift side of the SPAW however remains parallel to the coast and has not welded to the coast. The alongshore variability has increased, with multiple rips that have formed on both sides of the SPAW. The rip current on the leeward side of the SPAW is still present with a relatively low intensity. In the last timestep the SPAW has totally welded to the inner sandbar and therefor the coast. The rip current at the leeward side of were the SPAW welded is still present.

4.3.3 Alongshore variability

Figure 21 shows the relationship between the width of a SPAW and the evolution of the alongshore profile at the cross-shore location of X= 160m. Hereby it is clear that a SPAW is a perturbation to the nearshore morphodynamics. Whereas a relatively regular rip spacing can be observed for the no SPAW base case this is not the case for the simulations with a SPAW. For all the cases it can be observed that the rips migrate in the leeward direction over time. However, this occurs in higher extent for the no SPAW base case and the simulation including a SPAW with a width of 100m. While the simulation with SPAWs of respectively 300m and 500m in width tend to stick to their location. The first alterations in the elevation present itself at an earlier stage for the simulation with an increased width. For the wider SPAW this occurs around 20 hours, while this is approximately 35 hours for the SPAWs with a width of 100 and 300m. For the no SPAW base case this occurred around 40 hours. Accordingly, the formation of the rips occurred at an earlier stage for the wider SPAW, where these were present at around 50 hours. This occurred around 65 hours for the no SPAW base case, with the smaller SPAWs the

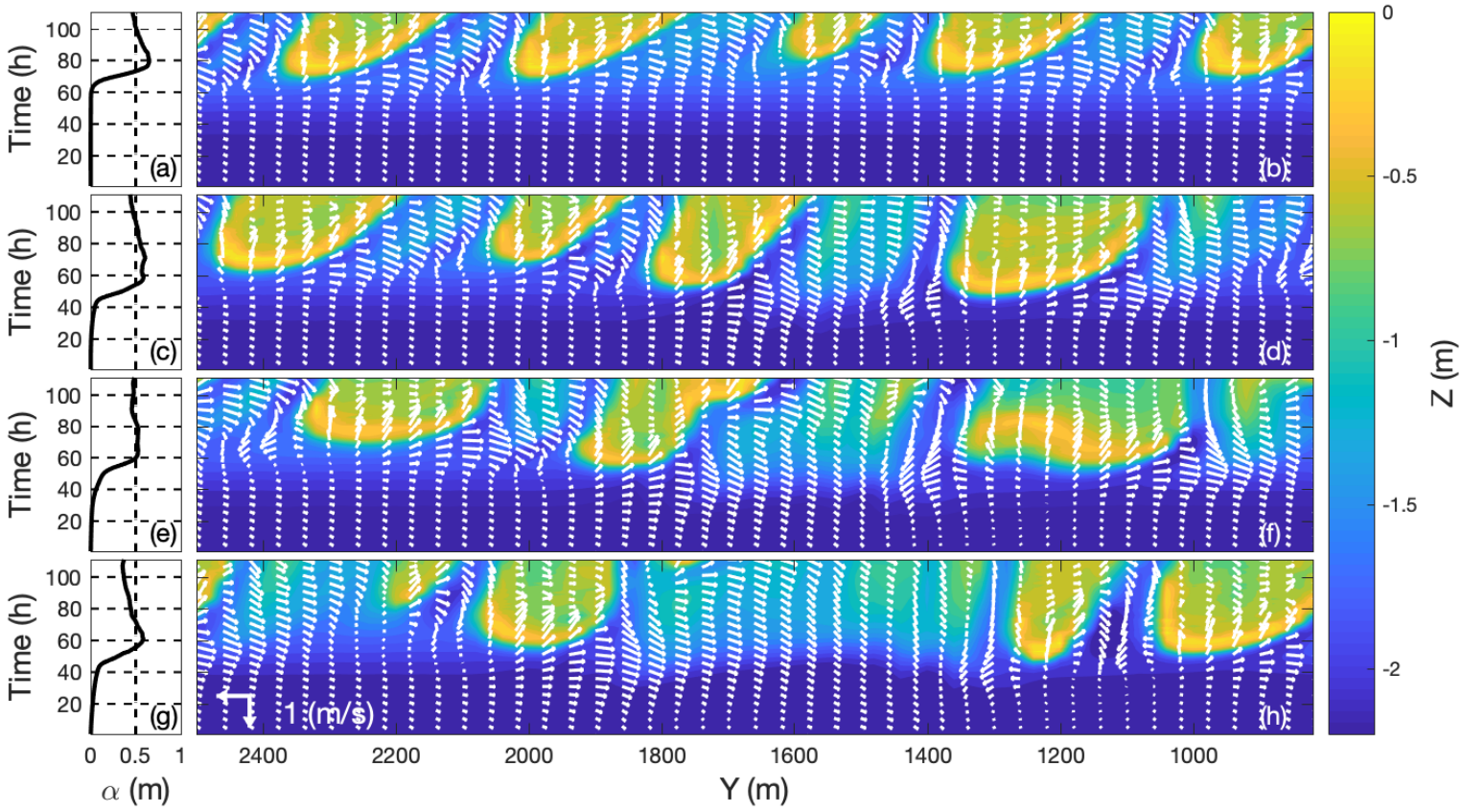

Figure 21 The evolution of the alongshore profile and alongshore variability at 160m cross-shore distance through time with the arrows indicating the modeled currents (a) for the no SPAW base case, (b) a SPAW with a width of 100m (c) for the base case with a width of 300m and (d) a SPAW with a width of 500m. The colorbar indicates the elevation in meters. Currents facing the bottom indicate an offshore directed current.

timestep of 55 hours. For all the case including SPAWs the gradual welding to the inner sandbar is visible. The narrowing of the SPAW however is only visible for the SPAWs with a width of 100 and 300 meters. This coincides with the timing of the completion of the welding which occurs at an earlier stage for the SPAW with a smaller width than for the wider SPAW. Additionally, the rip pattern becomes less consistent with increasing width of the SPAW. The highest magnitudes of the currents for all the simulations with a SPAW are found at the sides of the SPAW with an oblique onshore direction at the beginning of the welding. Hereafter the magnitude decreases over time. Furthermore, at the simulation of the SPAW with a width of 300 and 500m that the current over the SPAW decreases in the leeward alongshore direction with respect to the angle of wave incidence.

When these outcomes are compared to the root mean square error of an alongshore profile, it can be seen that for all the cases including a SPAW the alongshore variability gradually increases from timestep 20, for the SPAW with a width of 500m an increase can be seen from the start of the simulation. Where the alongshore variability of the simulations with a width of 100m and 500m increase rapidly at approximately 45 hours this occurs for the SPAW base case at 50 hours. Subsequently the alongshore variability of the simulations with a width of 100m and 500m peak at 0.6, while the SPAW base case stops at 0.5. Furthermore, the SPAW base case stays at 0.5, while the simulation including the SPAW with a width of 100m gradually decreases from 0.6 to 0.5. The wider SPAW with a width of 500m decreases gradually to 0.4. For the no SPAW base case the alongshore variability increases at a later stage than for all the simulations including a SPAW.

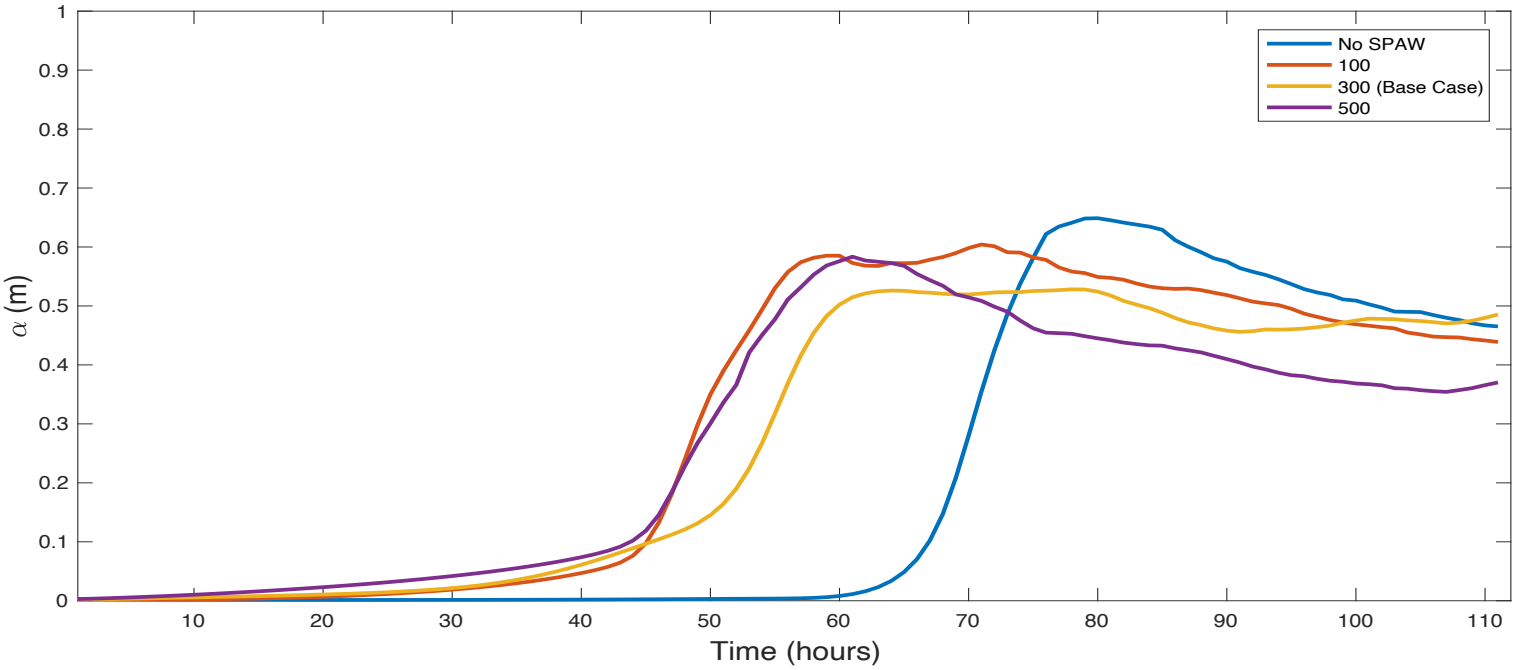

Figure 22 The evolution of the alongshore variability at 160m cross-shore distance through time, for the simulation for a SPAW with a width of 100m, 300m (Base Case) and 500m.

4.3.4 Volume of the nearshore zone

Figure 23 shows the evolution of the volume of the defined nearshore zone through time for simulation with a varying width of the SPAW. There is a clear relation visible between the width of the SPAWs and the amount of volume in the nearshore zone at the end of the simulation. Where a wider SPAW results in more volume in the nearshore zone at the end of the simulation. Next to that the steep volume increase at the beginning

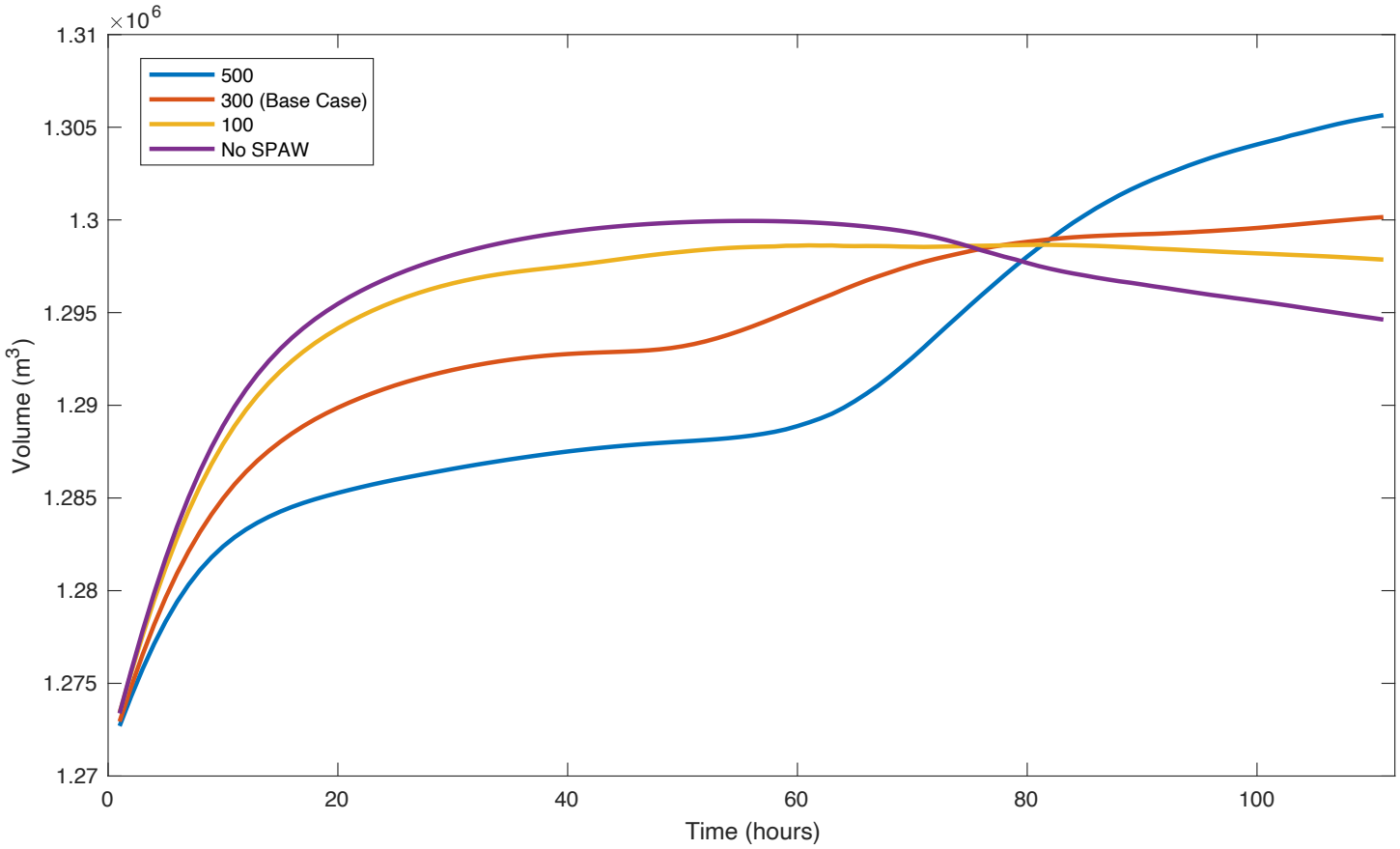

Figure 23 The evolution of the volume of the nearshore zone through time, for the simulations varying the width of the SPAW from 100m, 300m up to 500m and the no SPAW base case.

of the simulation is less intense for the wider SPAW and that the volume stabilizes for all the case at approximately 25 hours. After that for the SPAW base case a second moment of volume increase start around 50 hours, while this occurs for the SPAW with a width of 500m at approximately 60 hours. The second moment of increase is characterised by a steeper increase for the wider SPAW then for the SPAW base case. At the same moment the SPAW with a width of a 100m maintains its volume and the no SPAW base case starts to gradually decrease. This results in an intersection of all the lines between 75 and 80 hours. After this intersection all lines keep their gradient and result in higher end volumes for the simulations with a wider SPAW.

4.4 Wave incidence

Multiple simulations were executed with a wide variety in the angle of wave incidence. In this Chapter one extreme simulation is discussed in detail, with an angle of wave incidence of 40°.

4.4.1 Morphodynamics of a SPAW with oblique incoming waves

Figure 24 shows the migration of a SPAW with a similar the dimension and cross-shore location as the SPAW base case, however enduring waves with an incidence of 40°. Therefor the initial image looks very similar to the SPAW base case in Figure 11, which the exception that the circular currents that were located at the tips of the SPAW are now located a little further in the leeward direction. In the next timestep the SPAW has migrated in an onshore oblique direction. Furthermore, the elevation gap in the inner sandbar is not located at the same alongshore location as the SPAW but is located leeward of the SPAW which is due to the oblique incoming waves. The circular currents

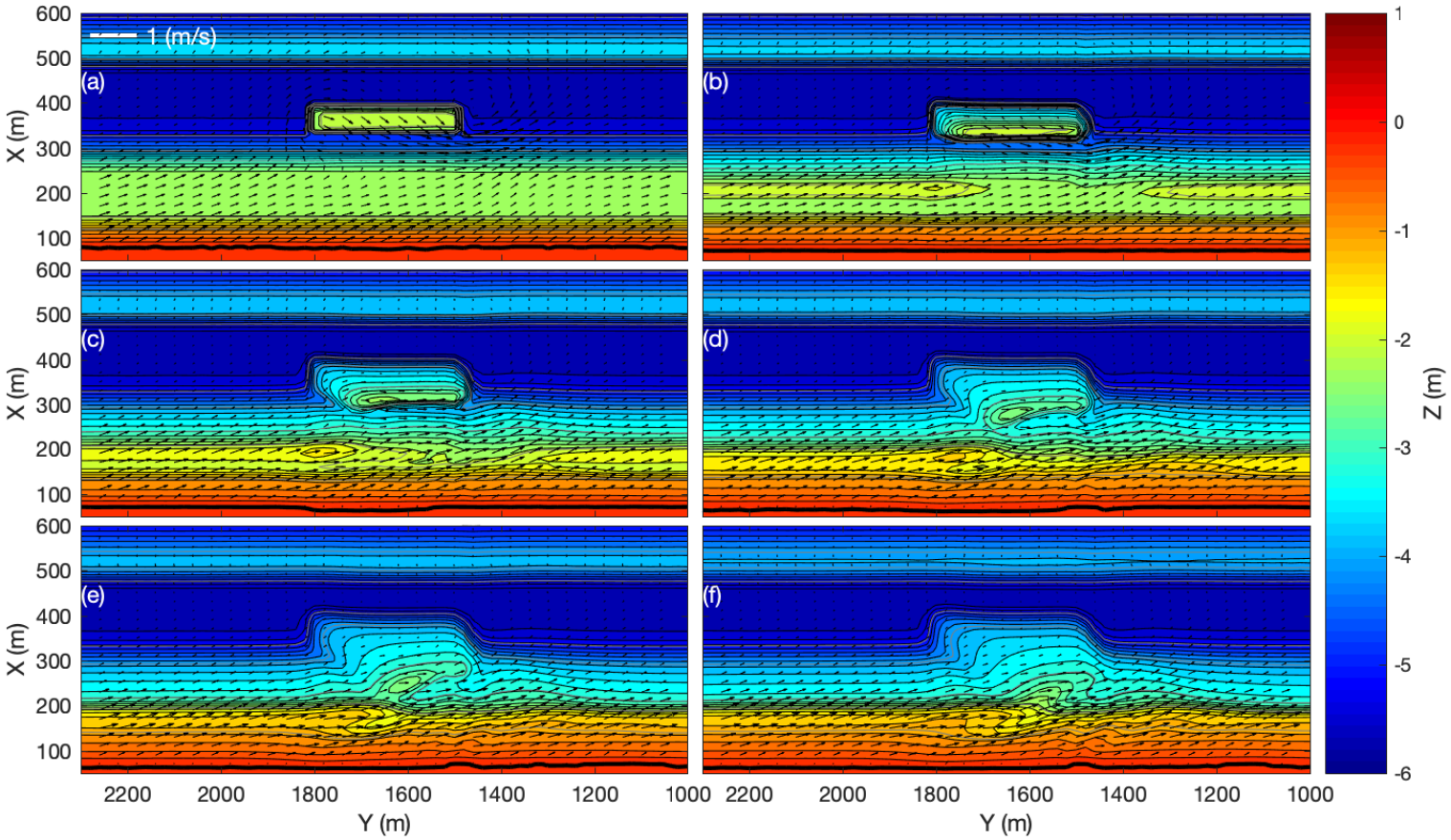

Figure 24 Top view of morphodynamic evolution of the coast and with the arrows indicating the modeled currents for a SPAW with the same dimensions and location as the SPAW base case, but an angle of wave incidence of 40°, at timestep a) 2 hours b) 20 hours c) 40 hours d) 60 hours e) 80 hours and f) 100 hours. The wave forcing consists of a wave height of 1.5m, a wave period of 8s and an angle of wave incidence of 40°.The color bar shows the seabed elevation in meters and the dark line indicates the mean sea level shoreline.

at the windward side is absent while the circular current at the updrift side of the SPAW is still present. The rip current at the leeward side of the SPAW has originated. In Figure 24c the SPAW has migrate obliquely further in the onshore direction. At the same time the size of the SPAW has decreased substantially and that the updrift side has the most elevated area. In the next timestep the updrift side of the SPAW has tilted in the onshore direction. The inner sandbar has migrated in the onshore direction but does not show signs increasing alongshore variability. The elevation gap and the rip current remain present. In Figure 24e the updrift side of the SPAW has welded to the coast, while this occurs in Figure 24f for the leeward side. After the SPAW has welded to the coast, there is a minimal amount of alongshore variability with only the rip current remaining present as a distinctive feature.

Figure 25 shows the erosion and accretion patterns due to currents, wave action, traditional component and combined together for the simulation with an angle of wave incidence of 40° for four different timesteps. It can be observed that in the first timestep for all the components there is an onshore directed transport of the SPAW. Where for the wave action component there is an additional onshore directed transport at the shoreline. At the same location there is an offshore directed transport for the wave driven component. In the second timestep the gravitational and current driven component have relatively small values. The current component shows minimal action around the SPAW, while the wave action component clearly visualises the onshore directed transport of the SPAW and inner sandbar. Although the area of the SPAW has decreased with respect to the first timestep. Due to the low values of the gravitational and current components the total sediment transport has a high similarity with the wave

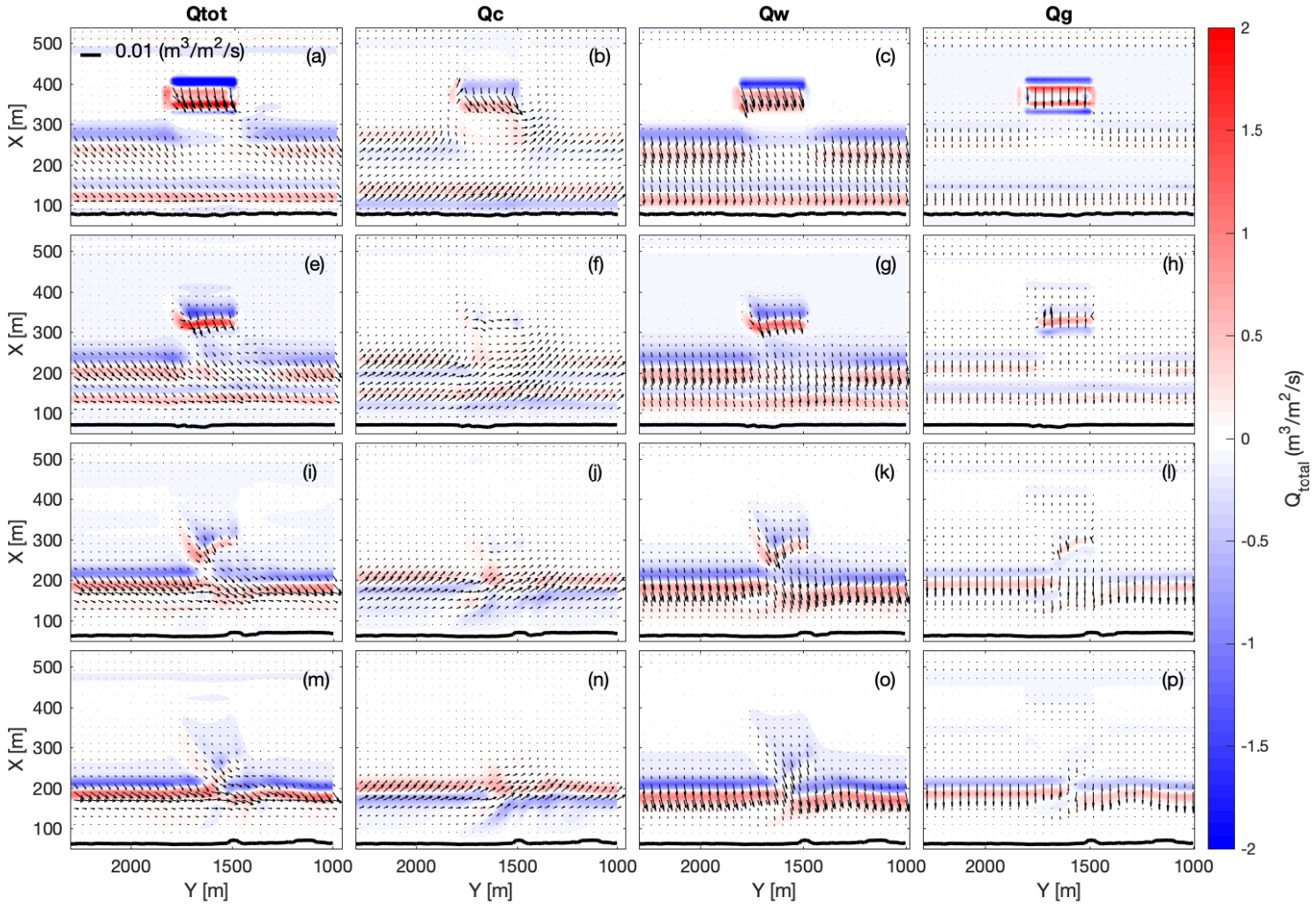

Figure 25 Erosion/accretion patterns for the simulation with an angle of wave incidence of 40° driven by the total sediment transport (first column) and the sediment transport due to currents (second column), wave action (third column), and the gravitational component (fourth column), with the arrows indicating the sediment fluxes. The first row (a-d) at 2 hours, second row (e-h) at 33 hours, the third tow (i-l) at 67 hours and the last row (m-p) at 100 hours. The colorbar shows the vertical change in seabed elevation in [m3/m2/s] and the dark line indicates the mean sea level shoreline.

action component for this timestep. Next to the updrift side of the SPAW accretion patterns are visible, which was not visible to this extent in Figure 13 for the SPAW base case. In the second timestep the gravitational and current driven component have relatively small values. The wave action component shows an onshore migration of a smaller SPAW area than in the previous timestep. The accretion/erosion areas are relatively V-shaped. The current driven component shows almost no action around the SPAW, while an offshore directed transport is seen at the inner sandbar. At the same time, an alongshore current is visible at the inner sandbar.
In the last timestep a similar image as the previous timestep is visible with the gravitational component having an onshore directed transport of the inner sandbar while the current driven component has an offshore directed transport at the inner bar cancelling each other out. This results in a total sediment transport that is very similar to the wave action component, which shows minor onshore transport of the SPAW.

When looking at the various migration paths for the differing scenarios with respect to the angle of wave incidence it can be observed that the migration path is more oblique with respect to the coast when the angle of wave incidence is higher. Additionally, the cross-shore travelled distance is less for a higher angle of wave incidence. For the beginning of the simulations regarding 10° and 20° the location of the highest point of the SPAW seems to wander off to the right before it proceeds to its final course

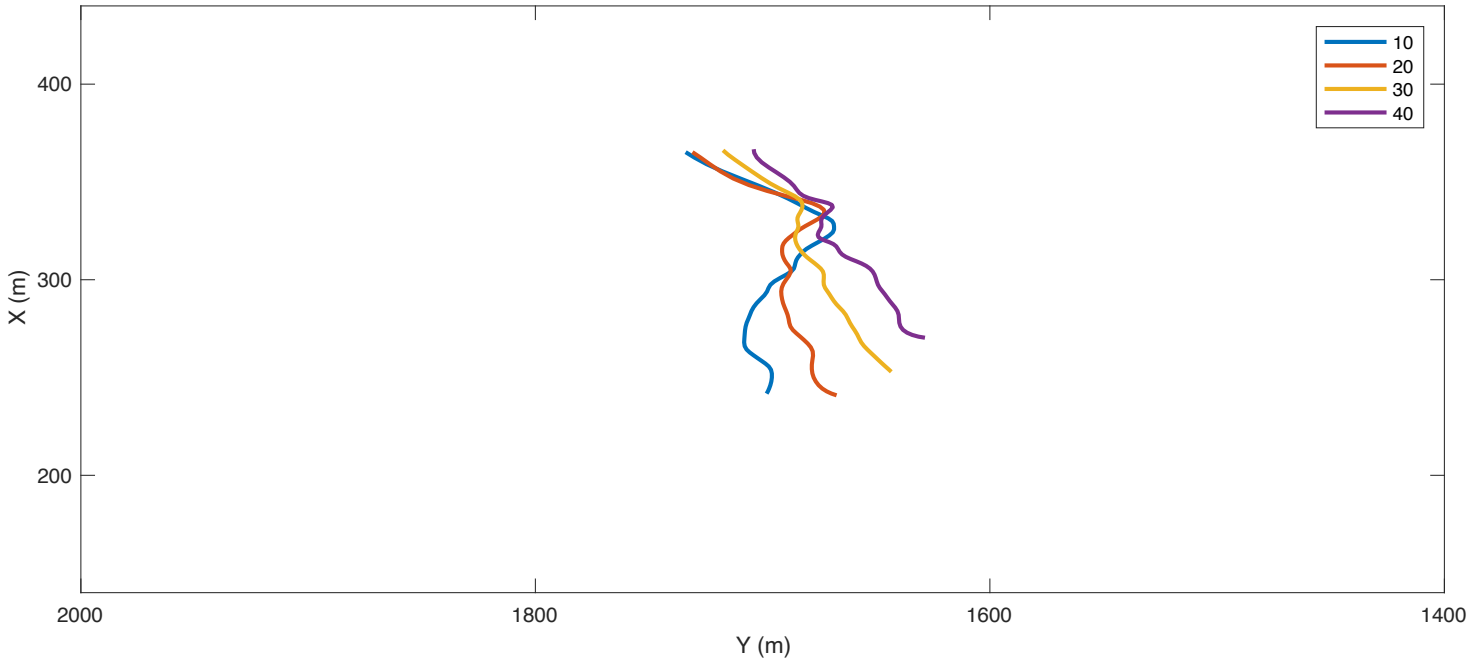

Figure 26 Migration paths of SPAWs for differing angles of wave incidence from 10° to 40° based on the highest point of the SPAW at each moment in time.

perpendicular to the shore. For the simulation regarding an angle of wave incidence of 30° and 40° this phenomenon is not as clearly present, and their migration paths are relatively constantly oblique with respect to the shoreline.

4.4.2 Alongshore variability

Figure 27 shows the evolution of the alongshore profile located at 160m cross-shore distance through time for simulations with an angle of wave incidence of 0°, 15° and 40°. Three strikingly different evolutions of an alongshore profile can be observed in Figure 27. Whereas for the simulation with an angle of wave incidence of 0°, shows a symmetric image including small alongshore variations from the beginning of the simulation, which was not noticed in any other simulation. Furthermore, at approximately 35 hours the alterations due to the presence of the SPAW are witnessed. At the alongshore location of the SPAW a gradual elevation increase is visible until the end of the simulation, with the highest values in the center. At roughly 50 hours rips start to form alongside more elevated areas. These more elevated areas coincide with horns of the inner sandbar and maintain their alongshore location through the whole simulation. Additionally, these areas have a relative stable elevation after their origination. The two rips which are located next to the SPAW remain at the same location through the simulation and keep their elevation. While the rips at respective alongshore location of 1000 and 2300m maintain their location but have an increase in elevation over time. The currents in the simulation with an angle of wave incidence of 0° are symmetrical and have the highest magnitude at the sides of the SPAW during the beginning of the welding. Where for the SPAW base case relatively significant currents are witnessed over the SPAW this is not the case for simulation with an angle of wave incidence of 0°. Where the currents with a higher magnitude are located solely at the rips. For the simulation with an angle wave incidence of 40° at the timestep of 25 hours the first alterations in the elevation can be noticed. After that moment until approximately 50 hours across the whole profile an elevation increase can be seen. After this period an elevation gap is visible at respective alongshore location of 1700 to 1400m, with the less elevated area around 1500m. This location coincides with location of the rip witnessed in Figure 24. This elevation gap narrows over time especially on the updrift side. For the currents it can be seen that during the whole simulation there is an alongshore uniform alongshore current, which is

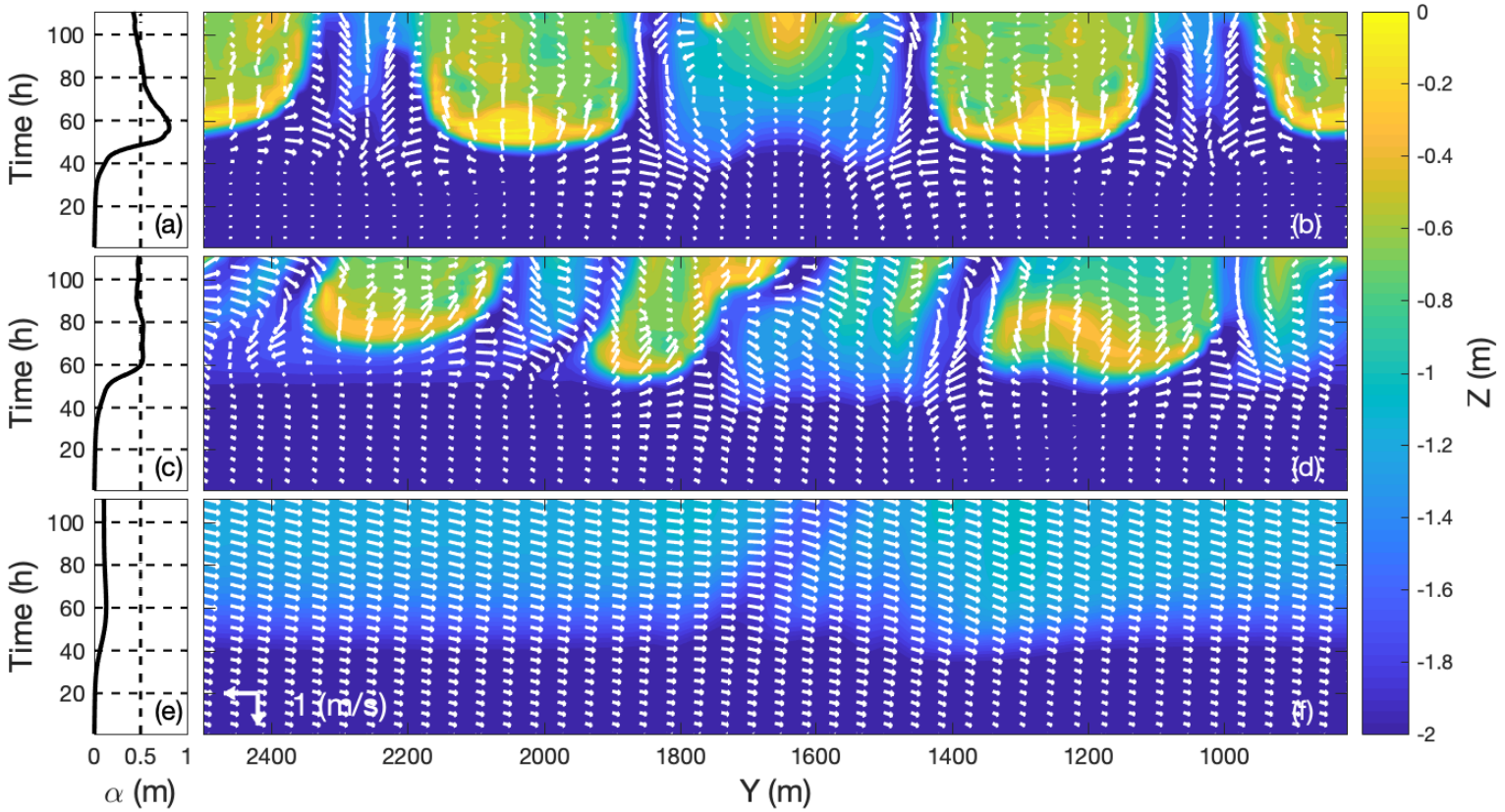

Figure 27 The evolution of the alongshore profile and the alongshore variability at 160m cross-shore distance through time with the arrows indicating the modeled currents for the simulation an angle of wave incidence of (a--b) 0° (c-d) 15° (SPAW base case) (e-f) 40°. The colorbar indicates the elevation in meters. Currents facing the bottom indicate an offshore directed current.

slightly offshore directed. It can be seen in the singular rip that the current is slightly more offshore directed. For an extensive description of the simulation with an angle of wave incidence of 15° see chapter 4.1.3.

In general, an angle of wave incidence of 0° results in multiple rips maintaining their alongshore locations, 15° results in multiple rips which migrate in the leeward direction

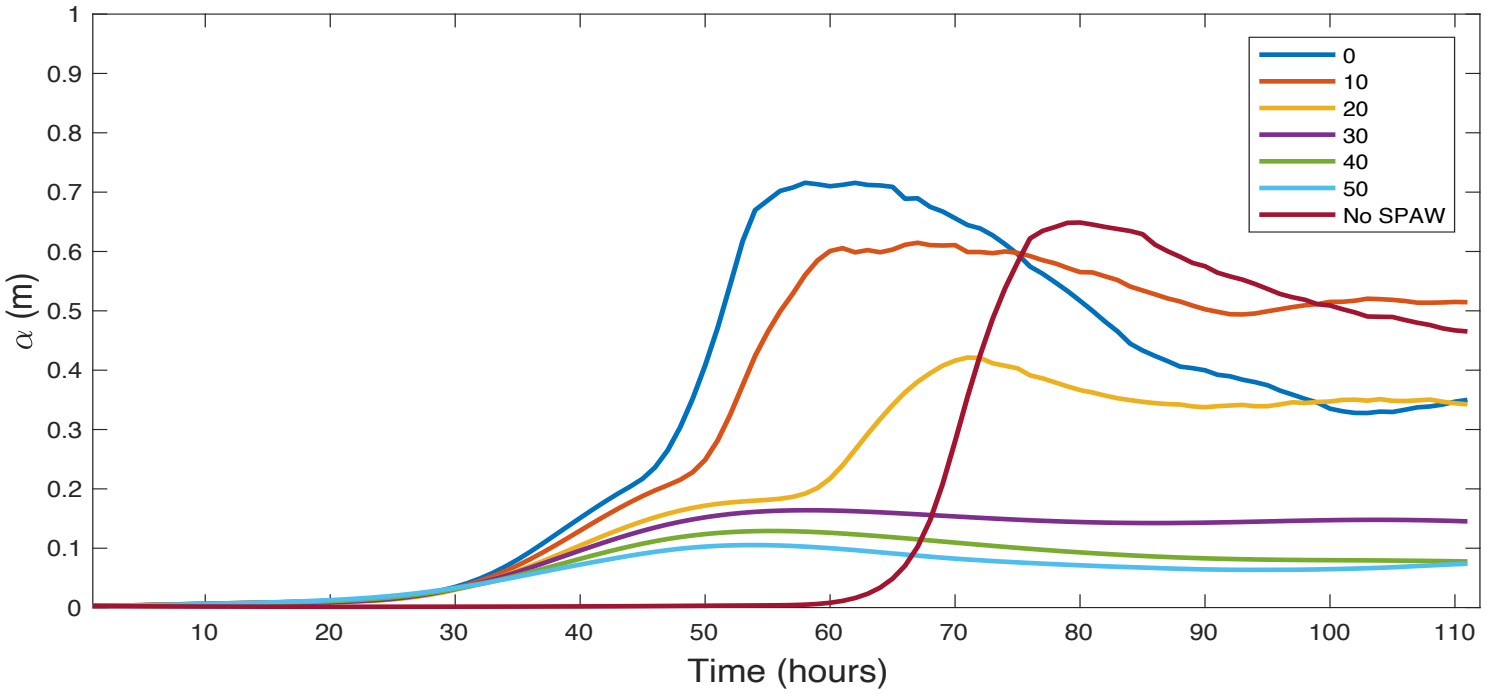

Figure 28 The evolution of the alongshore variability at 160m cross-shore distance through time, for the simulation with a varying angle of wave incidence from 0° up to 50° and the no SPAW base case with an angle of wave incidence of 15°.

with respect to the angle of wave incidence over time and 40° results in a singular rip on the leeward side of the SPAW which migrates in the leeward direction over time.

This is further illustrated in Figure 28 where can be seen that an increase in the angle of wave incidence results in a decrease in alongshore variability. Whereas all simulations except the no SPAW base case have a small alongshore variability since the timestep of 20 hours where after it gradually increases until 30 hours for all SPAW including simulations. After that the simulation with an angle of wave incidence of 0° results in the highest peak of alongshore variability, although it rapidly decreases afterwards. While the simulations with a higher angle of wave incidence remain relatively stable after their peak they peak at a lower point. When the angle of wave incidence is 30° or higher the alongshore variability does not peak anymore but remains at a very low point for the rest of the simulation. However, even at this stage a higher angle of wave incidence leads to a smaller alongshore variability while the temporal evolution of α remains the same.

4.4.3 Volume of the nearshore zone

There is a clear relation visible between the angle of wave incidence and the amount of volume in the nearshore zone at the end of the simulation, where a higher angle of wave incidence results in a lower volume of the defined nearshore zone. A higher angle of wave incidence results in a less intense increase in the beginning of the simulation. Additionally, the extra volume which coincides with the SPAW entering the defined nearshore zone is added more gradually for the simulations with a higher angle of wave incidence. For the cases with highest angle of wave incidence the simulation was not long enough to fully capture the welding of the SPAW to the coast.
For the simulation with an angle of wave incidence of 0° a dip in the volume can be seen at approximately 55 hours. This coincides with rips extending far offshore and therefor out of the boundary of the defined nearshore zone, this can be seen in Appendix B.

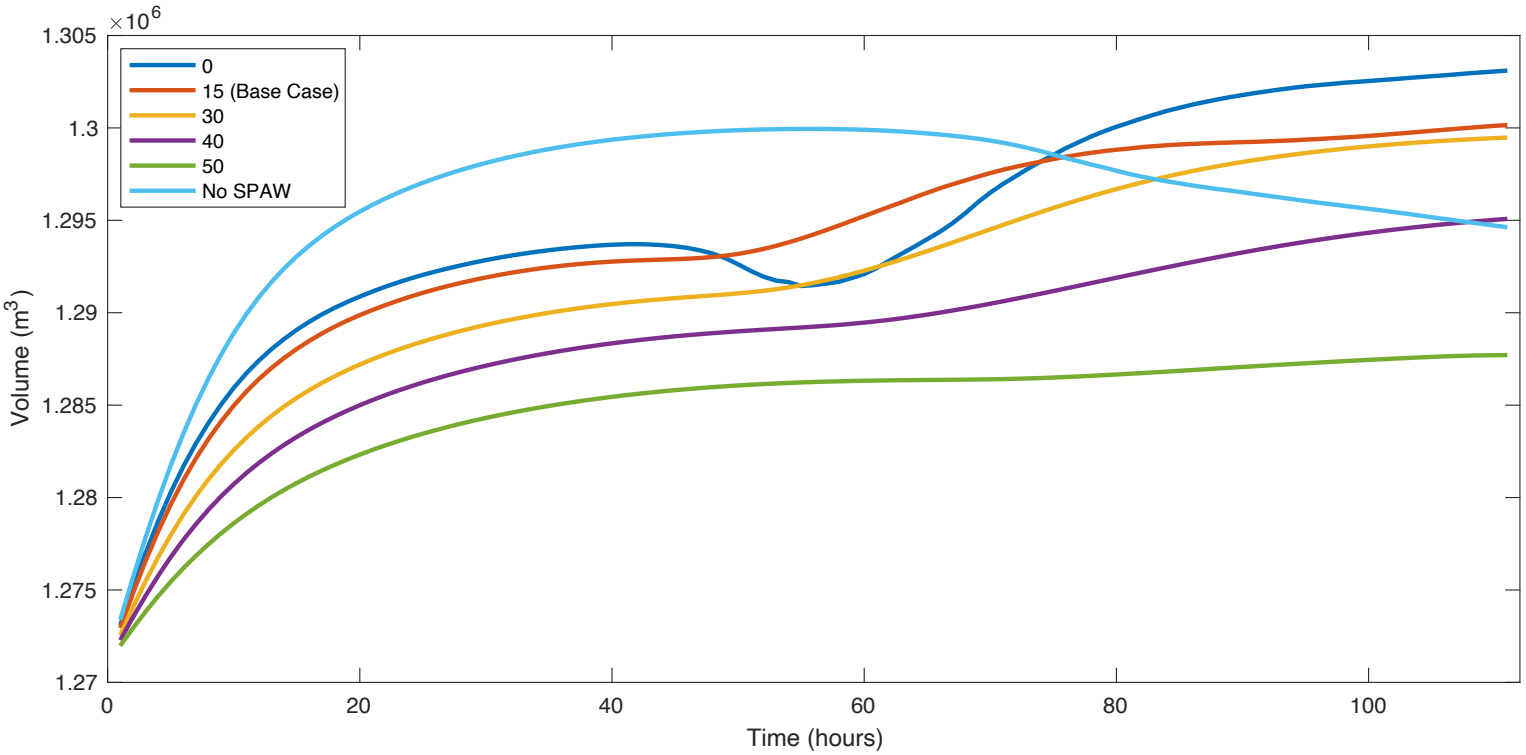

Figure 29 The evolution of the volume of the nearshore zone through time, for the simulations with a varying angle of wave incidence from 0° up to 50° and the no SPAW base case.

5. Discussion

5.1 SPAW morphodynamics

The variation of the cross-shore starting position gave new insights in the morphodynamic migration of the SPAW as this was unable to extract from observations. It can be seen in all the simulation that the SPAW leaves a trail of sediment, which rests at the elevation where the waves have no influence. By leaving a trail the SPAW loses sediment over time and with an increasing distance to the inner bar or shoreline the remaining volume of the SPAW decreases. Therefore, it is hypothesized that even though the wave conditions are favourable for the migration of a SPAW, if the cross-shore distance is too far or the through is too deep the SPAW is unable to reach the inner bar or shoreline as too much sediment is lost during the migration. If the SPAW does reach the inner bar or shoreline the amount of volume that the SPAW has at that moment defines the way the SPAW interacts with the existing bar-rip system. A more voluminous SPAW creates an energetic rip current at both sides of the SPAW simultaneously and create a new bar-rip system. While a small SPAW, on the other hand, that has lost most of its volume will solely be a nourishment for the existing bar-rip system. Furthermore, a further offshore located initial starting position results in a lower volume of the nearshore zone.
The variation of the dimension of the SPAW showed that a smaller SPAW migrates faster to the inner sandbar or shoreline than a wider SPAW. Furthermore, it showed that the wider SPAW did not break but migrated as a whole onshore. Where an elevation gap was always present in the inner sandbar regardless of the size of the SPAW. The elevation gap was substantially bigger during the simulation with a wider SPAW. It is hypothesized that this is due to the fact that waves break on the SPAW and therefor there is less wave energy to have an onshore transport at the inner bar. Additionally, this elevation gap resulted in a smaller volume increase of the nearshore zone in the beginning of the simulation as less sediment from the inner bar transported in the nearshore zone due to the decreased wave energy at this alongshore location.
The variation of the angle of wave incidence showed that a higher angle results in less sediment transport in the onshore direction. At the same time, a stronger alongshore current arises with a higher angle of wave incidence causing alongshore sediment transport. The combination of these two processes result in oblique migration path of the SPAW. This is unfavourable for the migration of a SPAW. Additionally, a higher angle of wave incidence results in less alongshore variability as the inner bar is straightened. This results in a singular rip current on the leeward side of the SPAW. Based on the chosen variables in this research the most sand reaches and remains in the defined nearshore zone, with a wide SPAW, located relatively onshore, during shore normal incoming waves. Where the nearshore morphodynamics are impacted most, with a base case sized SPAW, located relatively onshore, during slight obliquely incoming waves.

5.2 Onshore migration processes

This numerical modelling research of the migration of a SPAW shows a morphological development which is largely in line with observations (Wijnberg & Holman, 2007; Almar et al., 2010; Van Kuik, 2016; Korteling, 2017; Price, et al. 2017) and previous modelling study (Van der Weerd, 2012). As the model simulates a downstate sequence the development of crescentic bars would be expected, as the fact that sandbars would tend to migrate in the onshore direction (Van Enckevort, 2004; Van Maanen et al., 2008; Van de Lageweg et al., 2013; Castelle et al., 2010 (a); Price and Ruessink 2011). When looking at the outcomes of this research and the morphodynamic evolution of the coast during the simulations both these processes are in line with the previous studies. For the onshore migration of the SPAW it can be stated that the wave-non-linearity is the main

forcing while the circular currents at the tips have a minor influence on the onshore migration of the SPAW, this is in line with the findings by Van der Weerd, 2012. As a consequence, with a small wave height, no wave-non-linearity is present on top of the SPAW, which therefore is unable to migrate in the onshore direction. As the waves do not break on the SPAW it does not function as a perturbation and no imbalance between the pressure gradients and radiation stress is present resulting in the absence of currents around the SPAW.

5.3 Impact on nearshore morphodynamics

In the result section it can be seen that a SPAW generates an increase in sediment and functions as a natural nourishment to the coast. Furthermore, when the SPAW is in the vicinity of the inner bar it acts as a perturbation resulting in an elevation gap on the inner bar and a forceful rip current on the leeward side of the SPAW. Additionally, the SPAW seems to prevent the rip currents that arise from migrating in the leeward direction. Due to the fact that the SPAW acts as a perturbation, the coast is more dynamically active, resulting in a faster increase in α than a no SPAW case. However, this does not result in a higher alongshore variability at the end.

5.4 Model limitations

These findings provide new knowledge on the subject of the onshore migration of SPAWs in the nearshore zone and which morphological and wave conditions are favourable. As the model was unable to simulate the emergence of a SPAW with the chosen settings it was not possible to study the initiation of a SPAW. Secondly, the model was highly sensitive for variations of the wave period, with the chosen settings, so this could not be addressed. When the SPAW was exposed to waves with a wave height of 0.5m, the SPAW did not move, see Figure 30. Therefore, it can be stated that the migration of a SPAW is not a formality while using the model. It only migrates when it's exposed to the right conditions. The used bathymetry was not suited for high wave height values with the chosen setting as this resulted in numerical errors. On top of that time was limited to adjust the parameters of the model to make it suited for higher values of wave height. The model is limited for shoreline evolutions it was there for unable to research how a SPAW influences the shoreline dynamics.

5.5 Recommendations

Further study is required to provide more insight in how a SPAW initiates and which processes are dominant. However therefor a model is needed which can mimic the upstate sequence in bar morphology. Field studies will be necessary to confirm the presence of a trail behind the SPAW as this is not witnessed during observational research. Moreover, further study will be required to see to what extent the trail of sand at the areas the SPAW has migrated across will erode and vanish due to high wave heights or strong alongshore currents. Additionally, the fact that rip currents tend to maintain their position during the presence of a SPAW is worthwhile for further study. Just as modelling SPAW morphodynamics under time-varying wave conditions, including tides and modelling for different field sites.

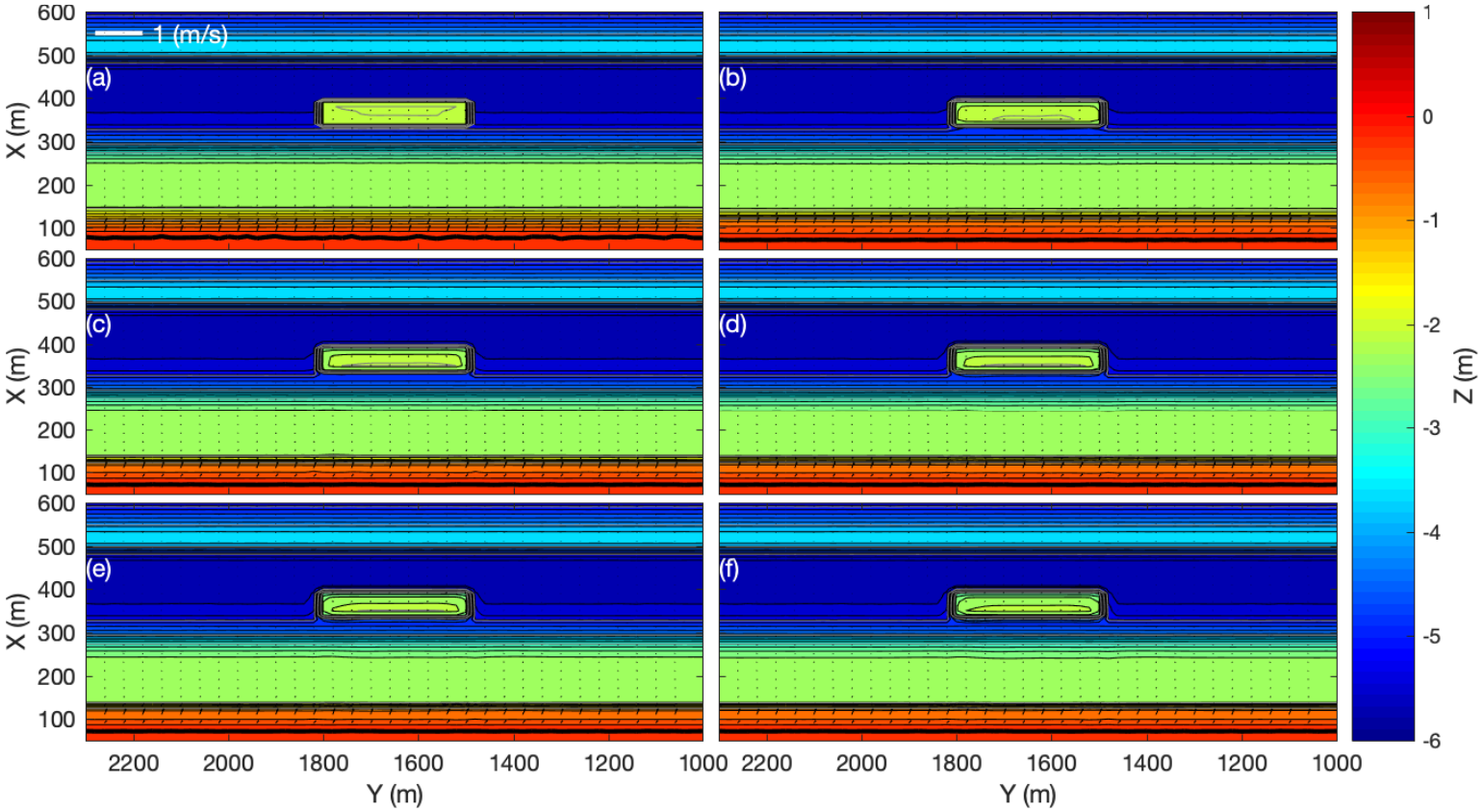

Figure 30 Top view of morphodynamic evolution of the coast and with the arrows indicating the modeled currents for a SPAW with the same dimensions and location as the SPAW base case, but with a wave height of 0.5m, at timestep a) 2 hours b) 20 hours c) 40 hours d) 60 hours e) 80 hours and f) 100 hours. The wave forcing consists of a wave height of 0.5m, a wave period of 8s and an angle of wave incidence of 15°.The color bar shows the seabed elevation in meters and the dark line indicates the mean sea level shoreline.

6. Conclusions

Using the nonlinear morphodynamic model 2Dbeach, implemented with a synthetic bathymetry derived from a bathymetric survey of the coast of Egmond aan Zee, this research aimed to explore which processes dominate the morphodynamics of the onshore migration of a SPAW and to resolve this subject the subsequent sub questions were formulated and answered.

What processes dominate the onshore migration of a SPAW during low energetic conditions?

The SPAW does not migrate during low energetic conditions as the waves are not high enough to break on the SPAW. As the waves do not break on the SPAW it does not function as a perturbation and no imbalance between the pressure gradients and radiation stress is present resulting in the absence of currents around the SPAW.

What is the role of wave-non-linearity (skewness and asymmetry) during the onshore migration of a SPAW?

Wave-non-linearity was the dominant factor in the onshore migration of the SPAW during the simulations.

What is the role of circulatory currents during the onshore migration of a SPAW?

The circular currents at the tips of the SPAW provided sediment fluxes but did not contribute significantly to the onshore migration of the SPAW.

How does the angle of wave incidence affect the onshore migration of a SPAW?

A higher angle of wave incidence is not favourable for the onshore migration of a SPAW, due to the alongshore current and coinciding oblique migration path. Moreover, the angle of wave incidence had dramatic results regarding the alongshore variability where shore normal wave resulted in a symmetrical shoreline with multiple rips, a slight angle of wave incidence resulted multiple rips with a less structural rip spacing and a high angle of wave incidence resulted in a singular rip and minimal alongshore variability.

How does the width of a SPAW influence the onshore migration?

The dimensions of the SPAW did not influence the processes regarding the onshore migration of the SPAW. However, a larger SPAW did need a longer period of time to migrate onshore.

How does the cross-shore position of the SPAW influence the onshore migration?

New insights were formed with respect to the trail of sand at the area the SPAW has migrated across as this was not observed prior to this study. This implies that the SPAW loses sand over time, while migrating onshore. Therefore, a further offshore cross-shore position acts negatively to the migration success of a SPAW. On this the hypothesis is made that even though the wave conditions are favourable for the migration of a SPAW if the cross-shore distance is to far or the through is to deep the SPAW is unable to reach the inner bar or shoreline as too much sediment is lost during the migration.

What impact does the presence of a SPAW have on the nearshore morphology?

If the SPAW does reach the inner bar or shoreline the amount of volume that the SPAW has at that moment defines the way the SPAW interacts with the existing bar-rip system. A more voluminous SPAW creates an energetic rip current at both sides of the SPAW simultaneously and create a new bar-rip system. While, a small SPAW, on the other hand, that has lost most of its volume will solely be a nourishment for the existing bar-rip system.

How does the presence of a SPAW influence the alongshore variability?

Due to the fact that the SPAW acts as a perturbation, the coast is more dynamically active, resulting in a faster increase in α than a no SPAW case. However, this does not result in a higher alongshore variability at the end.

Summarizing, the perfect conditions for a SPAW to bring sand onshore are shore normal or slightly oblique incoming waves, which have the height to break over the SPAW. For future research 2DBeach can provide a lot of answers regarding the simulations of SPAWs for different field sites, time-varying wave conditions or implementing tides. Furthermore, field studies will be necessary to confirm the presence of a trail behind the SPAW as this is not witnessed during observational research.

Almar, R., Castelle, B., Ruessink, B.G., Sénéchal, N., Bonneton, P. and Marieu, V. (2010). Two-and three-dimensional double-sandbar system behaviour under intense wave forcing and a meso–macro tidal range. *Continental Shelf Research*, 30(7) : 781-792.

Battjes, J. A., Janssen, J. P. F. M. (1978) Energy Loss and Set-Up Due to Breaking of Random Waves. *In Proceedings of the 16th Conference on Coastal Engineering, Hamburg, Germany, 27 August–3 September, American Society of Civil Engineers: New York, NY, USA,* pp. 569–587.53.

Battjes, J. A., Stive, M. J. F. Calibration and verification of a dissipation model for random breaking waves. *J. Geophys. Res.*1985,90, 9159.

Booij, N., R. C. Ris, Holthuijsen, L. H. (1999). A third-generation wave model for coastal regions: 1. Model description and validation, *J. Geophys. Res.*, 104(C4), 7649–7666.

Bouvier, C., Castelle, B., Balouin, Y. (2019). Modeling the Impact of Implementation of a Submerged Structure on Surf Zone Sandbar Dynamics. *J. Mar. Sci. Eng., 7,* 117

Bruneau, N., Bonneton, P., Castelle, B., Pedreros, R. (2011) Modeling rip current circulations and vorticity in a high-energy mesotidal-macrotidal environment. *J. Geophys. Res.*, 116, C07026

Castelle, B., Marieu, V., Bujan, S., Splinter, K.D., Robinet, A., Sénéchal, N. and Ferreira, S. (2015) Impact of the winter 2013–2014 series of severe Western Europe storms on a double-barred sandy coast: Beach and dune erosion and megacusp embayments. *Geomorphology*, 238: 135-148

Castelle, B., Marieu, V., Coco, G., Bonneton, P., Bruneau, N., Ruessink, B.G. (2012). On the impact of an offshore bathymetric anomaly on surf zone rip channels. *J. Geophys. Res.*, *117*, f1.

Castelle, B., Ruessink, B.G., Bonneton, P., Marieu, V., Bruneau, N., Price, T.D. (2010) Coupling mechanisms in double sandbar systems. Part 1: Patterns and physical explanation. *Earth Surf. Process. 35:* 476-486. (a)

Castelle, B., Bonneton, P., Sénéchal, N., Dupuis, H., Butel, R., Michel, D., (2006) Dynamics of wave-induced currents over an alongshore non-uniform multiple-barred sandy beach on the Aquitanian Coast, France. *Continental Shelf Research 26:* 113-131

Coco, G., Murray, B. G. (2007) Patterns in the sand: From forcing templates to self- organization. *Geomorphology, 91:* 271-290.

De Wit, L. (2017). Objective detection and quantitative analyses of a Shoreward Propagating Accretionary Wave in a double sandbar system (MSc Thesis). Utrecht University, 72p.

Dietrich, J.C., Zijlema, M., Allier, P.-E., Holthuijsen, L.H., Booij, N., Meixner, J.D., Proft, J.K., Dawson, C.N.,Bender, C.J., Naimaster, A., et al. (2013) Limiters for spectral propagation velocities in SWAN. *Ocean Model.* ,70, 85–102.

Dubarbier, B., Castelle, B., Ruessink, G., Marieu, V. (2017). Mechanisms controlling the complete accretionary beach state sequence. *Geophys. Res. Lett.*, *44*, 5645–5654.

Dubarbier, B., Castelle, B., Marieu, V., Ruessink, B. G. (2015). Process-based modelling of beach profile behavior, *Coastal Eng.*, *95*, 35–50.

Elias, E. P. L., Walstra, D. J. R., Roelvink, J. A., Stive, M. J. F. (2000) Hydrodynamic Validation of Delft3D with Field Measurements at Egmond. *In: Edge, B.L. (Ed.), Proc. 27th Int. Conf. on Coastal Engineering. ASCE, New York*, 2714-2727.

Gallagher, E. L., Elgar, S., Guza, R. T. (1998) Observations of sandbar evolution on a natural beach. *J. Geophys. Res.* 103,3203–3215

Giardano, A., Van der Werf, J., Van Ormondt, M. (2010) Simulating Coastal Morphodynamics with Delft3D: case study Egmond aan Zee. (Msc Thesis). Deltares Delft Hydraulics, 72p.

Greenwood, B., Davidson-Arnott, R. G. (1975). Marine bars and nearshore sedimentary processes, Kouchibouguac Bay, New Brunswick, Canada. *Nearshore sediment dynamics and sedimentation*, *16*, 123-150

Howd, P. A., Birkemeier, W. A. (1987) Beach and nearshore survey data: 1981–1984 CERC Field Research Facility. Tech. Rep. CERC-87-9. Coastal Engng. Res. Center, USAE Waterways

Hsu, T.-J., Elgar, S., Guza, R. T. (2006) Wave-induced sediment transport and onshore sandbar migration. *Coastal Eng.*, 53, 817-824

Konicki, K.M., Holman, R.A. (2000). The statistics and kinematics of transverse sandbars on an open coast. *Marine Geology, 169:* 69-101

Korteling, J. (2017) Natural Nourishments at the Gold Coast, Australia (Bachelor Thesis, University Utrecht)

Lippmann, T., Holman, R. (1990) The spatial and temporal variability of sand bar morphology. *J. Geophys. Res.* 95, 11575–11590

Mei, C., Stiassnie, M., Yue, D. (1989) Theory and Applications of Ocean Surface Waves: Part 1: Linear Aspects Part 2: Nonlinear Aspects. *World Scientific: Singapore*. Volume 23, p. 506.

Poate, T., Masselink, G., Russell, P., Austin, M. (2014) Morphodynamic variability of high-energy macrotidal beaches, Cornwall, UK. *Mar. Geol*. 350, 97–111.12C.

Price, T. D., van Kuik, N., de Wit, L., António, S., Ruessink, B.G. (2017). Shoreward propagating accretionary waves (SPAWs): Observations from a multiple sandbar system. *Coastal Dynamics,* 228: 1081-1089.

Price, T.D., Ruessink, B.G., Castelle, B. (2014) Morphological coupling in multiple sandbar systems – a review. *Earth Surf. Dynam., 2:* 309-321.

Price, T.D., Castelle, B., Ranasinghe, R., Ruessink, B.G. (2013) Coupled sandbar patterns and obliquely incident waves. *J. Geophys. Res., Earth Surf., 118:* 1677-1692.

Price, T. D., Ruessink, B. G. (2011). State dynamics of a double sandbar system. *Continental Shelf Research*, *31*(6), 659–674.

Ruessink, B. G., Ramaekers, G., Van Rijn, L. C. (2012) On the parametrization of the free-stream non-linear wave orbital motion in nearshore morphodynamics models. *Coastal Eng.*, 65, 56-63

Ruessink, B.G., Coco, G., Ranasinghe, R., Turner, I.L. (2007) Coupled and noncoupled behavior of three dimensional morphological patterns in a double sandbar system. *J. Geophys. Res., 112,* C07002

Ruessink, B. G., van Enckevort, I. M. J., Kingston, K. S., Davidson, M. A. (2000). Analysis of observed two- and three-dimensional nearshore bar behavior. *Marine Geology*, 169: 161-183

Ruessink, B.G. and Kroon, A. (1994) The behaviour of a multiple bar system in the nearshore zone of Terschelling, the Netherlands: 1965–1993. *Marine Geology*, 121(3), 187-197.

Rutten, J., Dubarbier, B., Price, T. D., Ruessink, B. G., Castelle, B. (2019) Alongshore Variability in Crescentic Sandbar Patterns at a Strongly Curved Coast. *Journal of Geophysical Research: Earth Surface*, 124

Shand, R.D. (2007). Bar splitting: system attributes and sediment budget implications for a net offshore migrating bar system. *Journal of Coastal Research*, 50: 72

Short, A.D. (1979) Wave power and beach-stages: a global model. *Proc 16th Int. Conf.Coastal Engineering,* Hamburg, pp. 1145–1162.

van der Weerd, L. (2012). Wave-driven dynamics of shoreward propagating accretionary waves in the nearshore (MSc Thesis). University of Twente/Deltares, 118p.

Van de Lageweg, W.I., Bryan, K.R., Coco, G. & Ruessink, B.G. (2013) Observations of shoreline-sandbar coupling on an embayed beach. *Marine Geology* 344, 101-114

Van Duin, M.J.P., Wiersma, N.R., Walstra, D.J.R., Van Rijn, L.C., Stive, M.J.F. (2004) Nourishing the shoreface: observations and hindcasting of the Egmond case, The Netherlands. *Journal of Coastal Engineering*, 51, 813-837.

van Enckevort, I. M. J., Ruessink, B. G., Coco, G., Suzuki., K., Turner, I. L., Plant, N. G., & Holman, R. A. (2004). Observations of nearshore crescentic sandbars. *Journal of geophysical research*, 109, C06028,

Van Enckevort, I.M.J., Ruessink, B.G. (2002) Video observations of nearshore bar behavior. Part 1: alongshore uniform variability. *Continental Shelf Research, 23:* 501-512. (a)

van Kuik, N. (2016). The effect of shoreface nourishments on Shoreward Propagating Accretionary Waves (Bachelor Thesis, University Utrecht).

Van Maanen, B., De Ruiter, P. J., Coco, G., Bryan, K.R., Ruessink, B. G. (2008) Onshore sandbar migration at Tairua Beach (New Zealand): Numerical simulations and field measurments. *Marine Geology* 253, 99-106

Wijnberg, K. M., Holman, R. A. (2007). Video-observations of shoreward propagating accretionary waves. *Proceedings of the RCEM* 2007: 737-743.

Wijnberg, K.M. (2002) Environmental controls on decadal morphologic behaviour of the Holland coast. *Marine Geology*, 189(3), 227-247.

Wright, L. D., Short, A. D. (1984) Morphodynamic variability of surf zones and beaches: asynthesis. *Mar. Geol.* 56 (1–4), 93–118

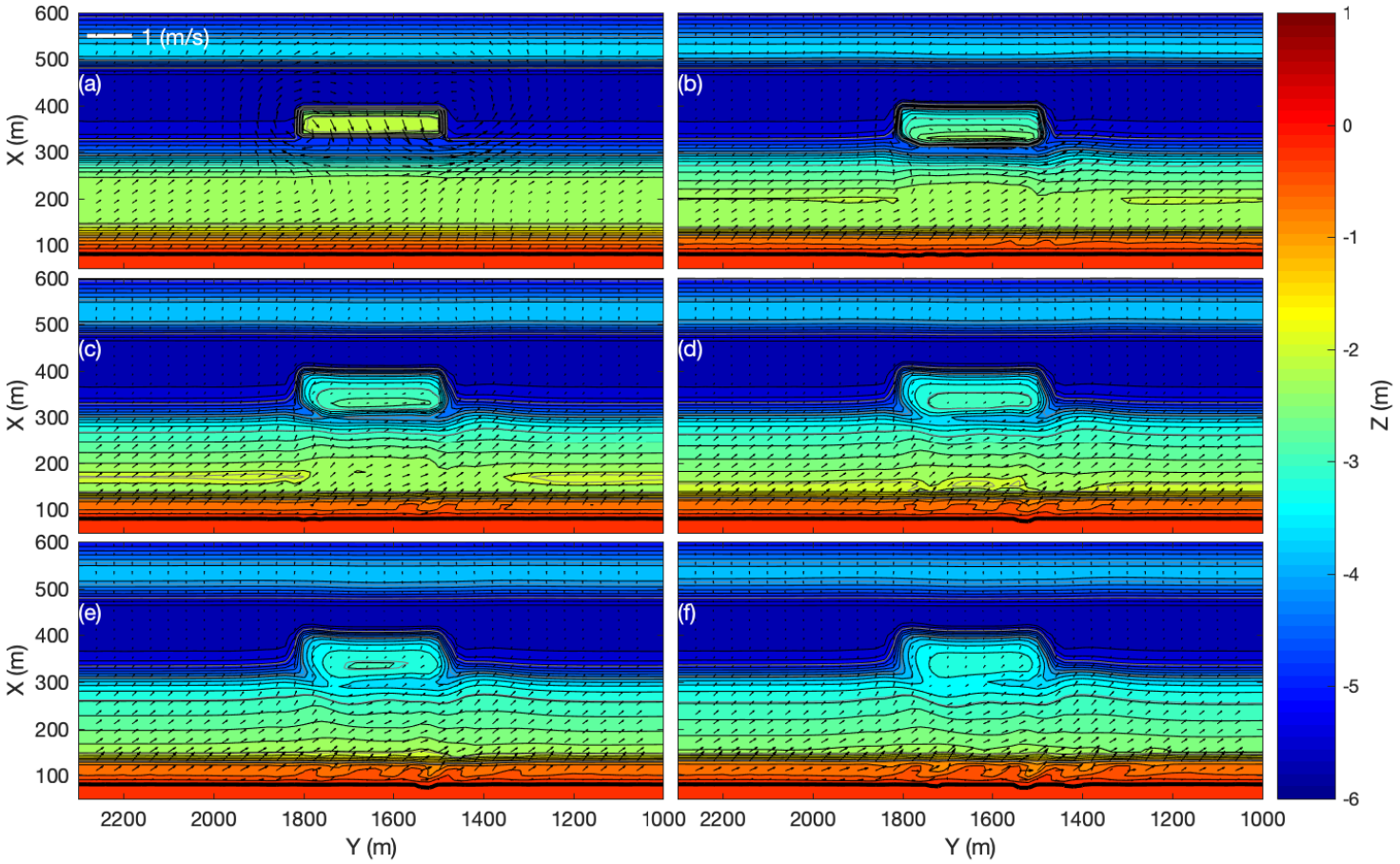

Appendix A Top view of morphodynamic evolution of the coast and with the arrows indicating the modeled currents for a simulation with a wave period f 6s, at timestep a) 2 hours b) 20 hours c) 40 hours d) 60 hours e) 80 hours and f) 100 hours. The wave forcing consists of a wave height of 1.5m, a wave period of 6s and an angle of wave incidence of 15°. The color bar shows the seabed elevation in meters and the dark line indicates the mean sea level shoreline

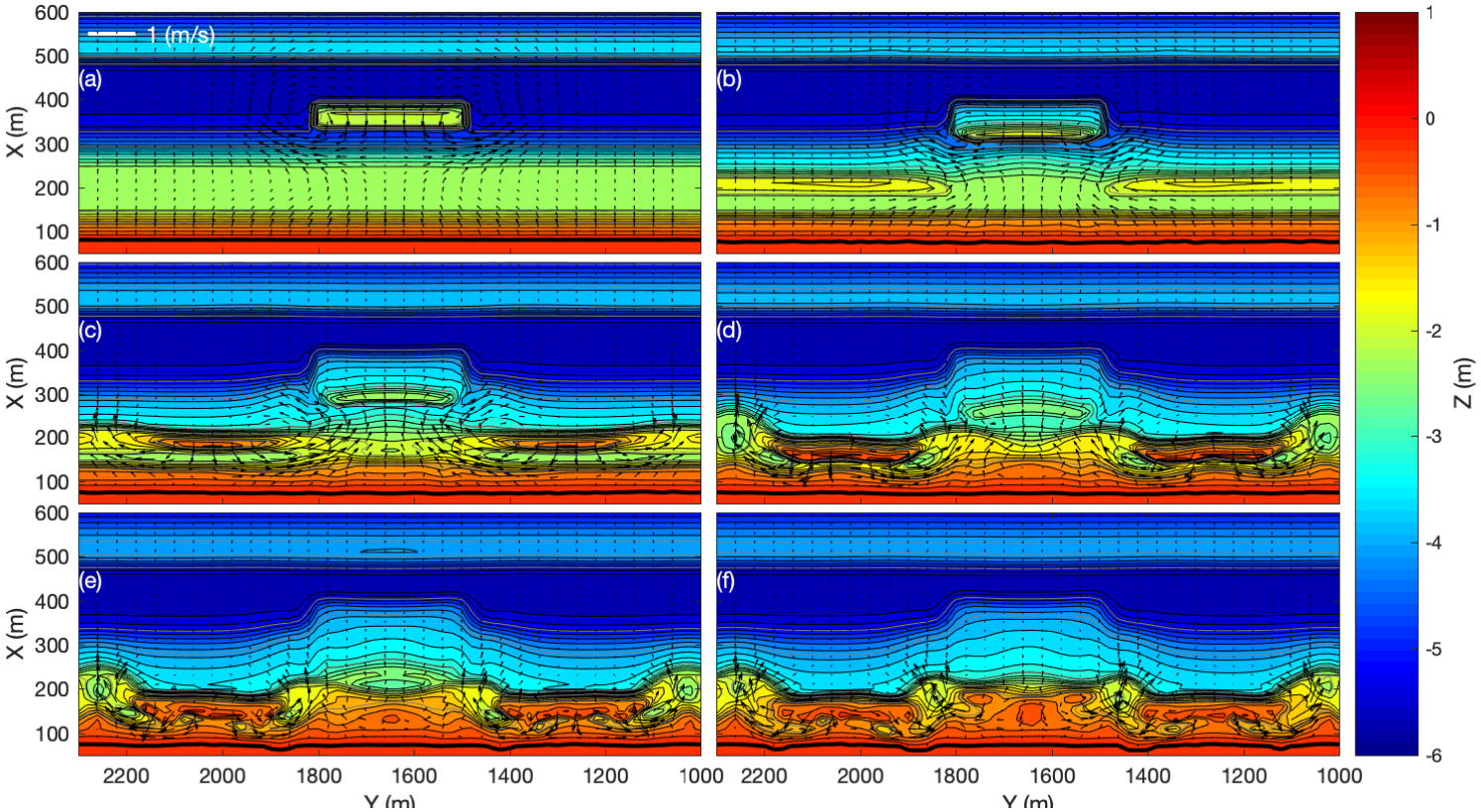

Appendix B Top view of morphodynamic evolution of the coast and with the arrows indicating the modeled currents for a simulation with an angle of wave incidence of 0°, at timestep a) 2 hours b) 20 hours c) 40 hours d) 60 hours e) 80 hours and f) 100 hours. The wave forcing consists of a wave height of 1.5m, a wave period of 6s and an angle of wave incidence of 0°. The color bar shows the seabed elevation in meters and the dark line indicates the mean sea level shoreline